Large twisting of non-circular cylinders in unconstrained elasticity

Federico Oyedeji Falope[1], Luca Lanzoni[2], Angelo Marcello Tarantino[3]

August 27, 2023

[1]DIEF, Università di Modena e Reggio Emilia, via P. Vivarelli 10, 41125, Modena, Italy, e-mail: federicooyedeji.falope@unimore.it,

[2]DIEF, Università di Modena e Reggio Emilia, via P. Vivarelli 10, 41125, Modena, Italy, e-mail: luca.lanzoni@unimore.it,

[3]DIEF, Università di Modena e Reggio Emilia, via P. Vivarelli 10, 41125, Modena, Italy, e-mail: angelomarcello.tarantino@unimore.it

Dedicated to Giuseppe Saccomandi sincere friend and distinguished colleague

Abstract

This paper deals with the equilibrium problem of non-circular cylinders subjected to finite torsion. A three-dimensional kinematic model is formulated, where, in addition to the rigid rotation of the cross sections, the large twist of the cylinder also generates in- and out-of-plane pure deformation of the cross sections and the variation of the cylinder length. Following the semi-inverse approach, the displacement field prescribed by the above kinematic model contains an unknown constant, which governs the elongation of the cylinder, and three unknown functions which describe the pure deformation of the cross sections. A Lagrangian analysis is then performed and the compressible Mooney-Rivlin law is assumed for the stored energy function. Once evaluated the Piola-Kirchhoff stresses, the boundary value problem is formulated. Nevertheless, the governing equations assume a coupled and nonlinear form which does not allow to apply standard solution methods. Therefore, the unknown functions are expanded into power series using polynomial terms in two variables. These series contain unknown constants which are evaluated applying the iterative Newton's method. With this procedure an accurate semi-analytical solution has been obtained, which can be used to compute displacements, stretches and stresses in each point of the cylinder. For the elliptical and rectangular sections, the results provided by the proposed solution

method are shown by a series of graphs. Finally, the Poynting effect was investigated by varying the section shape of the cylinder.

Keywords: Finite elasticity; Hyperelasticity; Compressible materials; Torsion; Warping function; Poynting effect.

1 Introduction

The key difference between a circular and a non-circular cylinder subjected to torsion is that while in the former case all cross sections remain plane when the cylinder is twisted, in the latter case these cross sections always undergo out-of-plane warping.

In the context of linear theory, the torsion of cylinders with (full) circular cross section was studied by Coulomb in 1784 [1]. This problem was then generalized to non-circular sections in Saint-Venant's impressive and fundamental work of 1855: *Mémoire sur la torsion des prismes* [2]. Saint-Venant was the first to understand the difference in deformation behavior between circular (the only one that does not warp) and non-circular sections. And the astonishment in him was so great that when he mentions the case studied by Coulomb he refers to it as the *old theory*. Using the semi-inverse method, Saint-Venant studied the equilibrium problem by considering a great variety of cross sections. In particular, he provided the solutions for the elliptical, rectangular, triangular bases and for sections with two orthogonal symmetries, whose contours are described by transcendental or algebraic functions. For the elliptical section, the solution is expressed in closed form. For the other sections, solutions are generally expressed by infinite polynomials or by series of exponential and transcendental functions. After twenty-four years, Saint-Venant returned to the case of the elliptical section in a brief note [3], obtaining formulae of great practical interest, still used today, for the determination of the unit angle of torsion and of the torsional stiffness of the cylinder.

The research undertaken by Saint-Venant for non-circular sections is still ongoing. In fact, it is easy to find recent papers on this subject in the Literature, where the problem is mainly tackled with numerical methods (see, for example, [4], [5], [6] and [7]).

When the torsional rotation is not very small, it is necessary to abandon the linear theory and formulate the problem in the fully nonlinear context of the finite elasticity. In this framework, however, only the case of circular cylinders has been treated. The main contributions were provided by Seth [8] in 1935 and by Rivlin [9], [10], and [11] in 1948-49. A detailed reconstruction of the historical development of the theory for circular cylinders is reported in [12]. Two well-known models were derived from Rivlin's studies: the pure torsion and the simple torsion, which are still used today. In simple torsion, after deformation, the cylinder retains its shape and volume. In pure torsion, the cylinder does not change its diameter. These models, even if they simplify the mathematical formulation of the torsion problem, are in contrast with Poynting's experiments [13], [14] and [15], according to which the length, diameter and volume of the

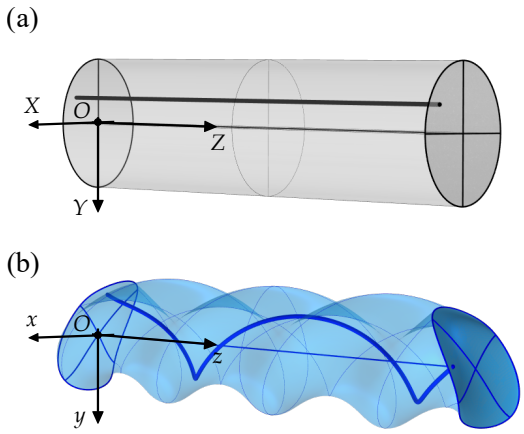

Figure 1: Deformation of a cylinder with elliptical base subjected to large torsion. (a) Initial configuration. (b) Final configuration generated by a twisting equal to 4π.

cylinder change. Recently, on the basis of the works of Poynting and Seth, the problem of torsion of circular cylinders has been tackled in [12], without assuming *a priori* kinematic and constitutive constraints. In this latest paper, it has been shown that, when a circular cylinder undergoes large twisting, it contracts transversely and extends longitudinally, changing its volume.

As already mentioned, no work formulated in the context of finite theory for non-circular cylinders seems to be found in the Literature. This may be due to the complexity of the mechanical phenomenon. To fix the ideas on the kinematic aspects, for example, observe the case illustrated in Fig. 1, where a cylinder with an elliptical section is twisted through an angle equal to 4π. In addition to rigidly rotating by a finite angle, cross sections exhibit pure deformation in and out (warping deformation) of their plane (the out-of-plane warping does not occur in the case of circular cylinders whose cross sections remain plane [12]). Furthermore, the solid changes its length. Note from Fig. 1b the intricate shape that the cylinder assumes after deformation.

This paper is organized as follows. Section 2 is devoted to the general formulation of the finite torsion problem for non-circular cylinders. On the basis of three physical assumptions, the shape of the displacement field is established. This field contains three unknown functions, which allow to evaluate the pure in-plane deformation of the sections and the warping function. Among the unknowns there is also the stretch of the torsion axis which governs the Poynting effect [13], [14] and [15]. By applying the material gradient operator to the displacement field, the deformation gradient tensor was obtained and then it was used in Section 3 to derive the Piola-Kirchhoff stress tensor. Then, assuming the compressible Mooney-Rivlin form for the stored energy function, the equilibrium problem is formulated. In Section 4, introducing the assumptions

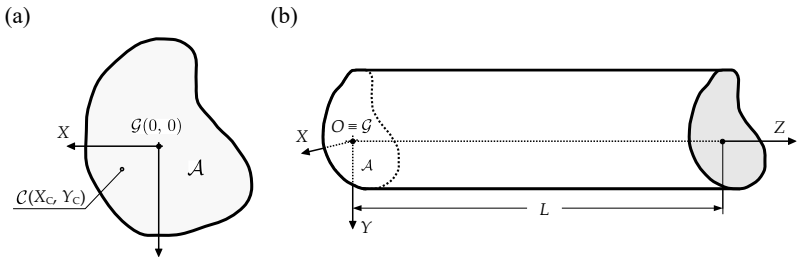

Figure 2: Non-circular cylinder $\bar{\mathcal{B}}$. (a) Torsional center and centroid of a generic cross section. (b) Undeformed configuration and reference system adopted.

of smallness of both deformations and displacements and a linear constitutive law, it is shown how the linearization of the boundary value problem yields the classical results of the linear theory. The governing equations are strongly nonlinear and coupled, therefore they cannot be solved with standard analytical methods. Therefore, in Section 5, a specifically devised solution techniques for this class of problems is presented. The three unknown functions are developed in power series through polynomial terms in two variables. All constants of the aforementioned three series are then evaluated by applying Newton's iterative method. Assessed the constants, semi-analytical expressions of the displacement field are obtained and, subsequently, deformation and stress tensors can be directly computed. The stresses thus determined can then be substituted into all the equations of the boundary value problem and a checking of the accuracy of the solution obtained can be carried out *a posteriori*. The applications for the elliptical section are carried out in Section 6, where the displacement field, stretches, Cauchy stresses and twisting moment, generated by varying the torsion angle, are calculated and shown in some graphs. As a special case also the circular section is investigated. In Section 7, what was done for the elliptical section is repeated for the rectangular section. In Section 8, it is shown how the shape of the cylinder section affects the Poynting effect. Section 9 closes the paper summarizing the results obtained.

2 General problem formulation

Let us consider a hyperelastic body composed of a homogeneous, isotropic and compressible material, having the shape of a right cylinder. The cross section $\mathcal{A}$ of the cylinder is assumed to be limited, compact and simply connected[1]. The shape of the cross section is left completely arbitrary, requiring only that its boundary $\partial\mathcal{A}$ be composed of sufficiently regular curves that meet without forming cusps (Lipschitz contour). No requirement of slenderness for the cylinder is introduced.

Reference is made to a Cartesian coordinate system $\{O, X, Y, Z\}$ having

[1]Dealing with multiply connected domains does not reserve particular difficulties.

the origin O positioned in the centroid of the left face of the body (see Fig. 2b). Thus, the body can be identified with the closure of the following regular region:

$$\mathcal{B} = \{(X, Y, Z) \mid (X, Y) \in \mathcal{A},\, 0 < Z < L\}$$

of the three-dimensional Euclidean space $\mathcal{E}$. The symbol L denotes the length of the cylinder. The cylinder axis coincides with the Z axis and all the centroids of the different cross sections belong to it.

The undeformed configuration $\bar{\mathcal{B}}$ of the body is assumed as the reference configuration, whereas the deformed configuration is given by the *deformation* $\mathbf{f}: \bar{\mathcal{B}} \to \mathcal{V}$.[2] The deformation $\mathbf{f}$ is a smooth enough, injective and orientation-preserving vector field (in the sense that $\det(\mathrm{Grad}\,\mathbf{f}) > 0$). The deformation of a generic material point P can be expressed by the well-known relationship

$$\mathbf{f}(P) = \mathbf{s}(P) + \mathbf{id}(P), \tag{1}$$

where $\mathbf{id}(P)$ and

$$\mathbf{s}(P) = u(P)\mathbf{i} + v(P)\mathbf{j} + w(P)\mathbf{k} \tag{2}$$

are the position and displacement vectors of the point P. In the vectorial equation (2), the functions $u(P)$, $v(P)$ and $w(P)$ denote the scalar components of $\mathbf{s}(P)$, whereas $\mathbf{i}$, $\mathbf{j}$ and $\mathbf{k}$ are the unit vectors. The application of the material gradient operator $\mathrm{Grad}(\cdot)$ to (1) gives

$$\mathbf{F} = \mathbf{H} + \mathbf{I}, \tag{3}$$

where $\mathbf{F} : \bar{\mathcal{B}} \to Lin^{+}$ and $\mathbf{H} : \bar{\mathcal{B}} \to Lin$ ([3]) are the deformation and displacement gradients, respectively. The symbol $\mathbf{I}$ denotes the identity tensor. In the following, a notation similar to that of the companion paper [12] will be used.

To derive the displacement field generated by the twisting of cylinders, four assumptions, which focus on the deformations that the cross sections can undergo, are described below.

1. Each cross section rotates rigidly around a point called torsional center $\mathcal{C}$, generally distinct from the centroid $\mathcal{G}$ (see, Fig. 2a)[4]. The torsional centers are aligned and belong to a line parallel to the axis of the cylinder, which remains rectilinear during twisting and which will be called torsional axis in the following. The rotation, characterized by a large angle, depends on the variable Z and is measured by the function $\theta(Z)$. Therefore, as the cylinder is twisted the longitudinal fibers, including the cylinder axis, are transformed into helices. This except the torsional axis that can only undergo length variations.

2. The longitudinal displacement $w(X, Y, Z)$ can be thought as consisting of two terms. The cross sections can translate rigidly along the Z axis, that is, all the points of a given cross section undergo the same longitudinal displacement.

[2] $\mathcal{V}$ is the vector space associated with $\mathcal{E}$.

[3] Lin is the set of all (second order) tensors whereas Lin^{+} is the subset of tensors with positive determinant.

[4] The coordinates of the torsional center X_c and Y_c are obtained from the condition $u = v = 0$.

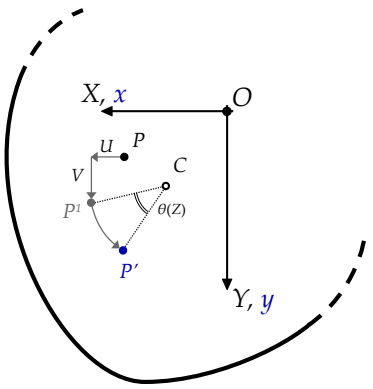

Figure 3: Composition of the displacements in the plane of a generic cross section.

This first contribution will be described by the function $f(Z)-Z$, and it governs the so-called *Poynting effect*. Once the position indicated by $f(Z)$ is reached, the cross sections undergo a further longitudinal displacement field, this time variable inside the cross sections. That is the cross sections warp. This second contribution is described by the warping function $\psi(X, Y)$. All the cross sections warp in the exact same way. Function ψ is sufficiently smooth and it vanishes at the torsional center, $\psi(X_c, Y_c) = 0$.[5]

3. The cross sections deform in their own plane all in the same way. Generally, this plane deformation is a non-uniform contraction that grows as one moves towards the outer edge. The two functions $U(X, Y)$ and $V(X, Y)$ are used to describe this latter deformation.[6]

4. Cross sections with two orthogonal axes of symmetry are considered.

On the basis of the transformations described in points 1 and 3, a generic material point $P(X, Y, Z)$ belonging to any cross section, identifiable by the variable Z, undergoes a plane displacement moving to $P^1(X+U, Y+V, Z)$. At the same time, a rigid rotation occurs and the point P^1 assumes the position $P'(X', Y', Z)$, where

$$\begin{cases} X' = (X + U - X_c)\cos\theta(Z) - (Y + V - Y_c)\sin\theta(Z), \\ Y' = (X + U - X_c)\sin\theta(Z) + (Y + V - Y_c)\cos\theta(Z). \end{cases} \tag{4}$$

These new variables, resulting from the finite rotation around the torsional center $\mathcal{C}$, are calculated by applying a two-dimensional orthogonal tensor. The composition of displacements just described which carries, within the same cross

[5] For the *restrained torsion problem* (studied in [12] for the case of circular cylinders): $f(Z) = Z$ and $\psi(X, Y) \equiv 0$ for any shape of the cross section. Since the longitudinal displacements w are prevented, cross sections do not warp and reactive stresses, varying inside the cross sections, arise.

[6] This third transformation quite complicates the mathematical formulation of the problem.

section, the point P in P' is illustrated by Fig. 3. Given the assumption in point 4, $X_c = Y_c = 0$ and the torsional center coincides with the centroid, $\mathcal{C} \equiv \mathcal{G}$. Simultaneously with the displacement above mentioned, the material point P undergoes an out-of-plane displacement, governed by the two functions ψ and f introduced at the point 2.

Based on the previous four assumptions, the displacement field can be derived by evaluating the final position occupied by a generic point $P(X, Y, Z)$

$$\begin{aligned} u(X, Y, Z) &= (X + U)\cos\theta(Z) - (Y + V)\sin\theta(Z) - X, \\ v(X, Y, Z) &= (X + U)\sin\theta(Z) + (Y + V)\cos\theta(Z) - Y, \\ w(X, Y, Z) &= \psi(X, Y) + f(Z) - Z. \end{aligned} \tag{5}$$

To twist the cylinder, the first cross section ($Z = 0$) can be fixed (retaining however the freedom to have a pure deformation), $\theta(0) = 0$, and a finite rotation α_0 can be prescribed to the final cross section ($Z = L$), $\theta(L) = \alpha_0$. In this situation, as shown in [12], a *uniform* state of torsion is generated along the axis of the cylinder (which is not altered by the non-linearities of the problem). It is then possible to attribute linear forms to the $\theta(Z)$ and $f(Z)$ functions:

$$\theta(Z) = \theta_1 Z, \quad \text{and} \quad f(Z) = CZ, \tag{6}$$

where $\theta_1 = \alpha_0/L$ is the twist angle for unit length and C is a constant to be determined (physically, it represents the stretch of the torsion axis).

For the finite torsion problem of non-circular cylinders, the displacement field (5), obtained on the basis of the kinematics described by the above four assumptions, contains three unknown functions, $U(X, Y)$, $V(X, Y)$ and $\psi(X, Y)$, and the unknown constant C, which will be determined in the sequel.

By applying the material gradient to (5) and using (3), the components of the deformation gradient $\mathbf{F}$ are calculated

$$\begin{aligned} [\mathbf{F}]_{11} &= (1 + U_{,X})\cos\theta_1 Z - V_{,X}\sin\theta_1 Z, \\ [\mathbf{F}]_{12} &= U_{,Y}\cos\theta_1 Z - (1 + V_{,Y})\sin\theta_1 Z, \\ [\mathbf{F}]_{13} &= -\theta_1\left[(X + U)\sin\theta_1 Z + (Y + V)\cos\theta_1 Z\right], \\ [\mathbf{F}]_{21} &= (1 + U_{,X})\sin\theta_1 Z + V_{,X}\cos\theta_1 Z, \\ [\mathbf{F}]_{22} &= U_{,Y}\sin\theta_1 Z + (1 + V_{,Y})\cos\theta_1 Z, \\ [\mathbf{F}]_{23} &= \theta_1\left[(X + U)\cos\theta_1 Z - (Y + V)\sin\theta_1 Z\right], \\ [\mathbf{F}]_{31} &= \psi_{,X}, \\ [\mathbf{F}]_{32} &= \psi_{,Y}, \\ [\mathbf{F}]_{33} &= C. \end{aligned} \tag{7}$$

Knowing the tensor $\mathbf{F}$, the right Cauchy-Green strain tensor $\mathbf{C} = \mathbf{F}^{\mathrm{T}}\mathbf{F}$ can

be evaluated directly

$$
\begin{array}{l}
[\mathbf{C}]_{11} = (1+U_{,X})^2 + V_{,X}^2 + \psi_{,X}^2, \\
[\mathbf{C}]_{12} = (1+U_{,X})\,U_{,Y} + (1+V_{,Y})\,V_{,X} + \psi_{,X}\psi_{,Y}, \\
[\mathbf{C}]_{13} = -\theta_1\,(1+U_{,X})\,(Y+V) + \theta_1\,(X+U)\,V_{,X} + C\psi_{,X}, \\
[\mathbf{C}]_{21} = [\mathbf{C}]_{12}\,, \\
[\mathbf{C}]_{22} = U_{,Y}^2 + (1+V_{,Y})^2 + \psi_{,Y}^2, \\
[\mathbf{C}]_{23} = -\theta_1\,(Y+V)\,U_{,Y} + \theta_1\,(X+U)\,(1+V_{,Y}) + C\psi_{,Y}, \\
[\mathbf{C}]_{31} = [\mathbf{C}]_{13}\,, \\
[\mathbf{C}]_{32} = [\mathbf{C}]_{23}\,, \\
[\mathbf{C}]_{33} = \theta_1^2\left[(X+U)^2 + (Y+V)^2\right] + C^2.
\end{array}
\tag{8}
$$

The tensor $\mathbf{C}$ is symmetric, $\mathbf{C} = \mathbf{C}^{\mathrm{T}}$, but it is not diagonal. This means that the reference system adopted is not principal. Orientation of the principal coordinate system varies with the point considered. It is important to note that the tensor $\mathbf{C}$ does not depend on the variable Z, since all the cross sections experience the same state of pure deformation.

The principal invariants of the tensor $\mathbf{C}$ are[7]

$$
\begin{array}{c}
I_1 = \| \mathbf{F} \|^2 = \mathrm{tr}\,(\mathbf{C}) = \\
(1+U_{,X})^2 + (1+V_{,Y})^2 + V_{,X}^2 + U_{,Y}^2 + \theta_1^2\left[(X+U)^2 + (Y+V)^2\right] \\
+\psi_{,X}^2 + \psi_{,Y}^2 + C^2,
\end{array}
$$

$$
\begin{array}{c}
I_2 = \| \mathbf{F}^\star \|^2 = \mathrm{tr}\,(\mathbf{C}^*) = \\
\left[(1+U_{,X})\,(1+V_{,Y}) - U_{,Y}V_{,X}\right]^2 + \left[(1+U_{,X})\,\psi_{,Y} - U_{,Y}\psi_{,X}\right]^2 \\
+\left[(1+V_{,Y})\,\psi_{,X} - V_{,X}\psi_{,Y}\right]^2 + \theta_1^2\left[(X+U)\,(1+U_{,X}) + (Y+V)\,V_{,X}\right]^2 \\
+\left[(1+U_{,X})\,C + \theta_1\psi_{,X}\,(Y+V)\right]^2 + \left[V_{,X}C - \theta_1\,(X+U)\,\psi_{,X}\right]^2 \\
+\theta_1^2\left[(X+U)\,U_{,Y} + (Y+V)\,(1+V_{,Y})\right]^2 + \left[U_{,Y}C + \theta_1\,(Y+V)\,\psi_{,Y}\right]^2 \\
+\left[C\,(1+V_{,Y}) - \theta_1\,(X+U)\,\psi_{,Y}\right]^2,
\end{array}
$$

$$
\begin{array}{c}
I_3 = (\det \mathbf{F})^2, \quad \text{with} \quad \det \mathbf{F} = \\
C\left[(1+U_{,X})\,(1+V_{,Y}) - U_{,Y}V_{,X}\right] + \theta_1\left[(Y+V)\,(1+V_{,Y}) + (X+U)\,U_{,Y}\right]\psi_{,X} \\
-\theta_1\left[(X+U)\,(1+U_{,X}) + (Y+V)\,V_{,X}\right]\psi_{,Y}.
\end{array}
\tag{9}
$$

3 Lagrangian stresses and formulation of the boundary value problem

Constitutive properties of a hyperelastic material are described by the stored energy function ω. If the function ω is frame-indifferent, homogeneous and isotropic, then it depends only on the principal invariants I_i, with $i = 1, 2$

[7]The following notations: $\| \mathbf{A} \| = \left(\mathrm{tr}\mathbf{A}^{\mathrm{T}}\mathbf{A}\right)^{1/2}$ for the tensor norm in the linear tensor space *Lin* and $\mathbf{A}^\star = (\det\mathbf{A})\mathbf{A}^{-\mathrm{T}}$ for the cofactor of the tensor $\mathbf{A}$ (if $\mathbf{A}$ is invertible) are used.

and 3. With these assumptions, the constitutive law ($\mathbf{T}_R = \partial\omega/\partial\mathbf{F}$) takes the following form:

$$\mathbf{T}_R = 2\left(\frac{\partial\omega}{\partial I_1} + I_1\frac{\partial\omega}{\partial I_2}\right)\mathbf{F} - 2\frac{\partial\omega}{\partial I_2}\mathbf{B}\mathbf{F} + 2I_3\frac{\partial\omega}{\partial I_3}\mathbf{F}^{-\mathrm{T}}, \tag{10}$$

where the tensor $\mathbf{T}_R$ denotes the (first) Piola-Kirchhoff stress tensor. In the above expression, $\mathbf{B} = \mathbf{F}\mathbf{F}^{\mathrm{T}}$ is the left Cauchy-Green strain tensor. Being $\mathbf{B}\mathbf{F} = \mathbf{F}\mathbf{C}$, this product can be calculated by means of (7) and (8). While the inverse of $\mathbf{F}$ is

$$\begin{aligned}
&\left[\mathbf{F}^{-1}\right]_{11}\det\mathbf{F} = C\left[U_{,Y}\sin\theta_1 Z + (1+V_{,Y})\cos\theta_1 Z\right]\\
&-\psi_{,Y}\theta_1\left[(X+U)\cos\theta_1 Z - (Y+V)\sin\theta_1 Z\right],\\
&\left[\mathbf{F}^{-1}\right]_{12}\det\mathbf{F} = -C\left[U_{,Y}\cos\theta_1 Z - (1+V_{,Y})\sin\theta_1 Z\right]\\
&-\psi_{,Y}\theta_1\left[(X+U)\sin\theta_1 Z + (Y+V)\cos\theta_1 Z\right],\\
&\left[\mathbf{F}^{-1}\right]_{13}\det\mathbf{F} = \theta_1\left[(X+U)\,U_{,Y} + (Y+V)\,(1+V_{,Y})\right],\\
&\left[\mathbf{F}^{-1}\right]_{21}\det\mathbf{F} = -C\left[(1+U_{,X})\sin\theta_1 Z + V_{,X}\cos\theta_1 Z\right]\\
&+\psi_{,X}\theta_1\left[(X+U)\cos\theta_1 Z - (Y+V)\sin\theta_1 Z\right],\\
&\left[\mathbf{F}^{-1}\right]_{22}\det\mathbf{F} = C\left[(1+U_{,X})\cos\theta_1 Z - V_{,X}\sin\theta_1 Z\right]\\
&+\psi_{,X}\theta_1\left[(X+U)\sin\theta_1 Z + (Y+V)\cos\theta_1 Z\right],\\
&\left[\mathbf{F}^{-1}\right]_{23}\det\mathbf{F} = -\theta_1\left[(X+U)\,(1+U_{,X}) + (Y+V)\,V_{,X}\right],\\
&\left[\mathbf{F}^{-1}\right]_{31}\det\mathbf{F} = \psi_{,Y}\left[(1+U_{,X})\sin\theta_1 Z + V_{,X}\cos\theta_1 Z\right]\\
&-\psi_{,X}\left[U_{,Y}\sin\theta_1 Z + (1+V_{,Y})\cos\theta_1 Z\right],\\
&\left[\mathbf{F}^{-1}\right]_{32}\det\mathbf{F} = -\psi_{,Y}\left[(1+U_{,X})\cos\theta_1 Z - V_{,X}\sin\theta_1 Z\right]\\
&+\psi_{,X}\left[U_{,Y}\cos\theta_1 Z - (1+V_{,Y})\sin\theta_1 Z\right],\\
&\left[\mathbf{F}^{-1}\right]_{33}\det\mathbf{F} = (1+U_{,X})\,(1+V_{,Y}) - U_{,Y}V_{,X}.
\end{aligned} \tag{11}$$

Therefore, having $\mathbf{F}$, $\mathbf{B}\mathbf{F}$ and $\mathbf{F}^{-1}$, the tensorial equation (10) provides the Lagrangian stress components. The expressions of each single component of the stress tensor $\mathbf{T}_R$ are reported in the Appendix.

Equilibrium requires that the following vectorial equation be satisfied locally:

$$\mathrm{Div}\mathbf{T}_R + \boldsymbol{b} = \boldsymbol{o}, \tag{12}$$

where $\mathrm{Div}(\cdot)$ denotes the material divergence and $\boldsymbol{b}$ the density of body forces in the undeformed configuration. This last function will be assumed equal to zero in the following.

To complete the mathematical formulation, the boundary conditions must be added to field equations (12). Boundary conditions can be imposed by requiring the lateral surface of the cylinder to be traction-free

$$\mathbf{t}_R = \mathbf{T}_R\,\mathbf{n}_{\mathbf{L}} = \boldsymbol{o}, \quad \text{for } \forall(X,\,Y) \in \partial\mathcal{A} \text{ and } \forall Z \in [0,\,L]\,, \tag{13}$$

where $\mathbf{t}_R$ denotes the Piola-Kirchhoff stress vector and $[\mathbf{n}_{\mathbf{L}}] = (\alpha_X,\,\alpha_Y,\,0)$, with $\alpha_X^2 + \alpha_Y^2 = 1$, the outward unit normal. Let $\Gamma(X,\,Y) = 0$ be the equation of the boundary of the cross section ∂A. Then, the direction cosines of $\mathbf{n}_{\mathbf{L}}$ are

$$\alpha_X = \frac{\frac{\partial\Gamma}{\partial X}}{\sqrt{\left(\frac{\partial\Gamma}{\partial X}\right)^2 + \left(\frac{\partial\Gamma}{\partial Y}\right)^2}}, \qquad \alpha_Y = \frac{\frac{\partial\Gamma}{\partial Y}}{\sqrt{\left(\frac{\partial\Gamma}{\partial X}\right)^2 + \left(\frac{\partial\Gamma}{\partial Y}\right)^2}}. \tag{14}$$

The boundary conditions on the two cylinder bases (i.e., for the two cross sections with $Z = 0$ and $Z = L$) are specified below. The initial cross section ($Z = 0$) does not rotate, $\theta(0) = 0$, and its torsional center does not move longitudinally $w(X_c, Y_c, 0) = 0$. The terminal cross section ($Z = L$) undergoes the prescribed overall torsional rotation α_0. Orthogonally, a static condition can be assigned by requiring that both end bases of the cylinder be free from normal stresses. This last condition is expressed as follows:

$$\mathbf{k} \cdot \mathbf{T}_R \, \mathbf{k} = 0, \quad \text{for } \forall (X, Y) \in \mathcal{A} \text{ and } Z = 0, \, L. \tag{15}$$

By writing of the field equations (12) and the boundary conditions (13) and (15), the formulation of the equilibrium boundary value problem for non-circular cylinders subjected to finite torsion can be considered formally completed.

To proceed it should now be assigned a specific law to the stored energy function ω. For it the compressible Mooney-Rivlin form is assumed:[8]

$$\omega(I_1, I_2, I_3) = a \, I_1 + b \, I_2 + c \, I_3 - (a + 2b + c) \, \ln I_3, \tag{16}$$

where the constants a, b and c are strictly positive quantities. It is well known that the above stored energy function, which depends on all three deformation invariants, describes properly the constitutive behavior of rubbers and rubber-like materials.[9] However, also with reference to other types of materials, other choices can be made by selecting different stored energy functions. Obviously, even with different choices of the energy ω, the analysis proposed in this paper can be applied. From (16) the following derivatives can be computed:

$$\omega_{,1} = a, \; \omega_{,2} = b, \; \omega_{,3} = c - \frac{a + 2b + c}{I_3}, \tag{17}$$

where $\omega_{,i} = \frac{\partial \omega}{\partial I_i}$, for $i = 1, 2$ and 3. With these three derivatives, the final form of the boundary-value problem is achieved. In particular, by substituting (17) into stress components (47) and then these into (12), the field equations in terms of displacement derivatives are obtained. These take the form of a coupled nonlinear system of three partial differential equations, with maximum degree equal to two. Similarly (47) and (17) must be introduced in the boundary conditions (13) and (15).

In the next Section 4, all the derived governing equations will be linearized, whereas in Section 5 a solving technique for the nonlinear boundary value problem, formulated in this Section, will be proposed.

4 Linearization of the mathematical formulation

In the present Section, invoking the hypotheses of smallness of both the deformation and displacement fields, the theory exposed in the previous Section 3

[8] This function is polyconvex and satisfies the growth conditions: $\omega \to \infty$ as $\lambda \to 0^+$ or $\lambda \to +\infty$. It was used, for example, in [16], [17], [18] and [19].

[9] For an extensive discussion of the terms related to the volume change in the stored energy function see the recent paper by M. Pelliciari et al. [20].

will be linearized, retrieving the classical results of the linear theory for non-circular cylinders subjected to torsion. In the linear theory, the torsional rotation $\theta(Z) = \theta_1 Z$ is very small and essentially regarded as an infinitesimal quantity.[10] In linear torsion, the cross sections rotate rigidly around the torsional center through an infinitesimal angle and do not undergo pure deformation in their own plane. Moreover, the cylinder axis does not change the length. Therefore, $U(X, Y) = V(X, Y) = 0$ and $C = 1$. The longitudinal displacements generated by the twisting of the cylinder are small and with them the warping function $\psi(X, Y)$ is also small. The following position for sake of convenience is introduced:[11]

$$\psi(X, Y) \simeq -\theta_1 \bar{\psi}(X, Y) + o(\theta_1), \tag{18}$$

where $\bar{\psi}$ and its partial derivatives $\bar{\psi}_{,X}$ and $\bar{\psi}_{,Y}$ are bounded functions. Based on the previous observations, the linearization of the displacement field (5) gives[12]

$$\begin{array}{c} u(X, Y, Z) \simeq -\theta_1 Y Z + o(\theta_1 Z), \\ v(X, Y, Z) \simeq \theta_1 X Z + o(\theta_1 Z), \\ w(X, Y, Z) \simeq \psi(X, Y) + o(\theta_1 Z). \end{array} \tag{19}$$

By applying the material gradient operator to (19) the linearized displacement gradient $\mathbf{H}$ is obtained[13]

$$[\mathbf{H}] \simeq \begin{bmatrix} 0 & -\theta_1 Z & -\theta_1 Y \\ \theta_1 Z & 0 & \theta_1 X \\ \psi_{,X} & \psi_{,Y} & 0 \end{bmatrix}. \tag{20}$$

Using the additive decomposition theorem, the tensor $\mathbf{H}$ can be split into its skw-symmetric part $\mathbf{W} = \frac{1}{2}\left(\mathbf{H} - \mathbf{H}^{\mathrm{T}}\right)$ and its symmetric part $\mathbf{E} = \frac{1}{2}\left(\mathbf{H} + \mathbf{H}^{\mathrm{T}}\right)$, that is $\mathbf{H} = \mathbf{W} + \mathbf{E}$,[14]

[10] Obviously, given the boundless of the length L, the density θ_1 is also an infinitesimal quantity.

[11] The Landau symbols are used.

[12] Using the Taylor series expansions, the following approximations are employed:

$$\sin\theta_1 Z \simeq \theta_1 Z + o(\theta_1 Z),$$
$$\cos\theta_1 Z \simeq 1 + o(\theta_1 Z).$$

[13] In the following the infinitesimals of higher order will be omitted.

[14] The following well-known definitions hold:

$$\omega_x = \frac{1}{2}\left(\frac{\partial w}{\partial y} - \frac{\partial v}{\partial z}\right), \quad \omega_y = \frac{1}{2}\left(\frac{\partial u}{\partial z} - \frac{\partial w}{\partial x}\right), \quad \omega_z = \frac{1}{2}\left(\frac{\partial v}{\partial x} - \frac{\partial u}{\partial y}\right),$$
$$\varepsilon_x = \frac{\partial u}{\partial x}, \quad \varepsilon_y = \frac{\partial v}{\partial y}, \quad \varepsilon_z = \frac{\partial w}{\partial z},$$
$$\gamma_{xy} = \frac{1}{2}\left(\frac{\partial u}{\partial y} + \frac{\partial v}{\partial x}\right), \quad \gamma_{xz} = \frac{1}{2}\left(\frac{\partial u}{\partial z} + \frac{\partial w}{\partial x}\right), \quad \gamma_{yz} = \frac{1}{2}\left(\frac{\partial v}{\partial z} + \frac{\partial w}{\partial y}\right).$$

$$[\mathbf{W}] = \begin{bmatrix} 0 & -\omega_z & \omega_y \\ \omega_z & 0 & -\omega_x \\ -\omega_y & \omega_x & 0 \end{bmatrix} \simeq \frac{1}{2} \begin{bmatrix} 0 & -2\theta_1 Z & -(\theta_1 Y + \psi_{,X}) \\ 2\theta_1 Z & 0 & (\theta_1 X - \psi_{,Y}) \\ (\theta_1 Y + \psi_{,X}) & -(\theta_1 X - \psi_{,Y}) & 0 \end{bmatrix}, \tag{21}$$

$$[\mathbf{E}] = \begin{bmatrix} \varepsilon_x & \frac{1}{2}\gamma_{xy} & \frac{1}{2}\gamma_{xz} \\ \frac{1}{2}\gamma_{xy} & \varepsilon_y & \frac{1}{2}\gamma_{yz} \\ \frac{1}{2}\gamma_{xz} & \frac{1}{2}\gamma_{yz} & \varepsilon_z \end{bmatrix} \simeq \frac{1}{2} \begin{bmatrix} 0 & 0 & -\theta_1 Y + \psi_{,X} \\ 0 & 0 & \theta_1 X + \psi_{,Y} \\ -\theta_1 Y + \psi_{,X} & \theta_1 X + \psi_{,Y} & 0 \end{bmatrix}. \tag{22}$$

Tensor $\mathbf{W}$ represents infinitesimal rigid rotations. As (21) shows, rotations are present at every point of the cylinder. Tensor $\mathbf{E}$ represents the infinitesimal strains. As (22) shows, the linearized strain state is biaxial and does not depend on Z.

Using (3), it is immediate to obtain from (20) the linearized deformation gradient[15]

$$[\mathbf{F}] \simeq \begin{bmatrix} 1 & -\theta_1 Z & -\theta_1 Y \\ \theta_1 Z & 1 & \theta_1 X \\ \psi_{,X} & \psi_{,Y} & 1 \end{bmatrix}, \tag{23}$$

Knowing the linearized tensor $\mathbf{F}$, the tensors $\mathbf{F}^{-1}$, $\mathbf{C}$, $\mathbf{BF}$ and the invariants I_1, I_2 and I_3, previously determined for the nonlinear theory, can be recalculated for the linear theory, getting [16]

$$\left[\mathbf{F}^{-1}\right] \simeq \begin{bmatrix} 1 & \theta_1 Z & \theta_1 Y \\ -\theta_1 Z & 1 & -\theta_1 X \\ -\psi_{,X} & -\psi_{,Y} & 1 \end{bmatrix}, \tag{24}$$

$$[\mathbf{C}] \simeq \begin{bmatrix} 1 & 0 & -\theta_1 Y + \psi_{,X} \\ 0 & 1 & \theta_1 X + \psi_{,Y} \\ -\theta_1 Y + \psi_{,X} & \theta_1 X + \psi_{,Y} & 1 \end{bmatrix}, \tag{25}$$

$$[\mathbf{BF}] = [\mathbf{FC}] \simeq \begin{bmatrix} 1 & -\theta_1 Z & -2\theta_1 Y + \psi_{,X} \\ \theta_1 Z & 1 & 2\theta_1 X + \psi_{,Y} \\ -\theta_1 Y + 2\psi_{,X} & \theta_1 X + 2\psi_{,Y} & 1 \end{bmatrix}, \tag{26}$$

$$I_1 = I_2 \simeq 3 \qquad \text{and} \qquad I_3 \simeq 1, \tag{27}$$

being $\det \mathbf{F} \simeq 1$. In addition, using (17), the constitutive quantities present in the Piola-Kirchhoff stress expression (10) reduce to

$$\begin{gathered} 2\left(\omega_{,1} + I_1\, \omega_{,2}\right) \simeq 2\left(a + 3b\right), \\ 2\omega_{,2} = 2b, \\ 2I_3\, \omega_{,3} \simeq -2\left(a + 2b\right). \end{gathered} \tag{28}$$

[15] The same tensor is obtained by linearizing the relations (7).

[16] Obviously, by linearizing the corresponding tensors and invariants of the previous Section, the same results are attained.

Given (10), (23), (24), (26) and (28), the linearized Piola-Kirchhoff stress tensor assumes the following form:

$$[\mathbf{T}_R] \simeq 2\,(a+b) \begin{bmatrix} 0 & 0 & -\theta_1 Y + \psi_{,X} \\ 0 & 0 & \theta_1 X + \psi_{,Y} \\ -\theta_1 Y + \psi_{,X} & \theta_1 X + \psi_{,Y} & 0 \end{bmatrix}. \tag{29}$$

This tensor is now symmetric and biaxial. As is well known, in the linear theory, the two measures of Lagrangian and Eulerian stress coincide. In fact, if the Cauchy stress tensor $\mathbf{T}$ is computed by means of its definition, $\mathbf{T}_R = (\det \mathbf{F})\,\mathbf{T}\mathbf{F}^{-\mathrm{T}}$, the same form of tensor (29) is achieved for it.

In the linear theory, as established in [16] (see also [21] and [22]), $2\,(a+b) = G$, where G is the first Lamè constant (or the shear modulus) and the twist angle for unit length θ_1 is usually expressed in the following form: $\theta_1 = q\frac{m_Z}{G\,I_p}$, where q is the torsion factor (it is dimensionless and depends solely on the shape of the cross section), I_p is the polar moment of inertia and m_Z is the external torque applied on the two bases of the cylinder and able to generate the overall rotation $\theta_1 L$.

Once the stress tensor (29) has been obtained, the linearized boundary value problem can be formulated. The material divergence of the linearized stress tensor (29) gives

$$[\mathrm{Div}\mathbf{T}_R] \simeq 2\,(a+b) \begin{bmatrix} 0 \\ 0 \\ \psi_{,XX} + \psi_{,YY} \end{bmatrix}. \tag{30}$$

The boundary condition on the lateral surface of the cylinder (13) becomes

$$[\mathbf{t}_R] \simeq 2\,(a+b) \begin{bmatrix} 0 \\ 0 \\ (-\theta_1 Y + \psi_{,X})\,\alpha_X + (\theta_1 X + \psi_{,Y})\,\alpha_Y \end{bmatrix} = \begin{bmatrix} 0 \\ 0 \\ 0 \end{bmatrix}, \tag{31}$$

where, setting $\alpha_X = \frac{dX}{dn}$ and $\alpha_Y = \frac{dY}{dn}$, the third component can be rewritten as

$$\frac{d\psi}{dn} = \frac{\partial \psi}{\partial X}\frac{dX}{dn} + \frac{\partial \psi}{\partial Y}\frac{dY}{dn} = -\theta_1 X \frac{dY}{dn} + \theta_1 Y \frac{dX}{dn}, \tag{32}$$

where $\frac{d\psi}{dn}$ denotes the directional derivative. The boundary condition (15), which requires that the normal stresses vanish at the end base of the cylinder, is automatically satisfied, since the normal stress $\mathrm{T}_{R_{33}}$ is even zero at every point of the cylinder. In conclusion, taking into account (30) and (32), the linearization of the nonlinear boundary problem (12), (13) and (15) provides

$$\begin{aligned} \Delta\psi &= 0, \\ \tfrac{d\psi}{dn} &= -\theta_1 X \tfrac{dY}{dn} + \theta_1 Y \tfrac{dX}{dn}, \end{aligned} \tag{33}$$

where the warping function ψ remains the only unknown function. The warping function usually employed in linear theory is $\bar{\psi}$, which is proportional to ψ, as

shown by (18). Therefore, using (18), the equilibrium problem (33) transforms into

$$\begin{aligned} \Delta\bar{\psi} &= 0, \\ \frac{d\bar{\psi}}{dn} &= X\frac{dY}{dn} - Y\frac{dX}{dn}. \end{aligned} \tag{34}$$

The classic linearized value problem, expressed by (34) in the mathematical form of a Neumann problem, must be solved by taking into consideration the particular shape of the cross section. Once the warping function $\bar{\psi}$ has been determined, the equilibrium problem of a non-circular cylinder subjected to torsion, in the context of linear theory, is solved. In fact, known $\bar{\psi}$, the displacements (19), the infinitesimal rigid rotations (21), the infinitesimal strains (22) and the stresses (29) can be computed in each point of the cylinder.

This Section can be concluded by observing that, through the linearization of the field equations and boundary conditions reported in Section 3, the classic boundary value problem for infinitesimal torsion of non-circular cylinders is fully retrieved.

5 Solving method

The solution of the equilibrium boundary value problem for non-circular cylinders subjected to finite torsion (in its general formulation given by field equations (13) and boundary conditions (14) and (16)) is the displacement field. Once this is known, in fact, the stretches and stresses at each point of the cylinder can then be calculated. Applying the semi-inverse method, the kinematics of the problem led directly to the displacement field (5), which can be thought of mathematically as a representation form of the equilibrium solution. The displacement field (5) contains three unknown functions, $U(X, Y)$, $V(X, Y)$ and $\psi(X, Y)$, and the unknown constant C. The two function $U(X, Y)$ and $V(X, Y)$ describe the plane pure deformation of the cross sections (the same for all cross sections of the cylinder). The function $\psi(X, Y)$ is the warping function, and it governs the variation of longitudinal displacement of each point of the cross section with respect to the longitudinal displacement of the torsional center. The constant C represents the stretch of the torsion axis. The three unknown functions, together with their partial derivatives, and the constant C appear in expressions of the Piola-Kirchhoff stresses (47). These stresses are used to enforce the boundary conditions (13) and (15). While to derive the field equations these stresses have to be derived further to calculate the divergence as required by the local equilibrium equations (12). The field equations thus take the form of a system of three partial differential equations of the second order in the three unknown functions U, V and ψ. This system is strongly nonlinear and coupled, in the sense that all the unknowns appear in each equation. Similar considerations also concern the boundary conditions. Obviously, ordinary analytical methods cannot be applied to this boundary value problem, therefore in the following to compute the displacement field we will have to resort to iterative numerical procedures.

From the mechanical nature of the considered equilibrium problem, it can be assumed that the unknown functions are very smooth and bounded. Moreover, the unknown functions are characterized by symmetry properties.[17] The function $U(X,\, Y)$ is an even function of the X coordinate and an odd function of the Y coordinate, while the converse is true for the function $V(X,\, Y)$. On the other hand, the warping function $\psi(X,\, Y)$ turns out to be skew-symmetric with respect both the X and Y axes. In addition, we can keep in mind that, when the twist angle α_0 is small, the linearized elastic solution, illustrated in Section 4, is a good tentative solution.

Taking into account the previous symmetry properties and assuming for the unknown functions a polynomial dependence on the Lagrangian coordinates, the following approximated general expressions are proposed:

$$\begin{aligned} U(X,\, Y) &\simeq \left(1 + a_{y1}Y^2 + a_{y2}Y^4 + ... + a_{yn}Y^{2n}\right)\left(a_{x1}X + a_{x2}X^3 + ... + a_{xm}X^{2m-1}\right) - X; \\ V(X,\, Y) &\simeq \left(1 + b_{x1}X^2 + b_{x2}X^4 + ... + b_{xn}X^{2n}\right)\left(b_{y1}Y + b_{y2}Y^3 + ... + b_{ym}Y^{2m-1}\right) - Y; \\ \psi(X,\, Y) &\simeq X\left(c_{11}Y + c_{12}Y^3 + ... + c_{1n}Y^{2n-1}\right) + X^3\left(c_{21}Y + c_{22}Y^3 + ... + c_{1n}Y^{2n-1}\right) + ...; \end{aligned} \tag{35}$$

with $n = 1, .., N$ and $m = 1, .., M$. The constants a_{yn}, a_{xm}, b_{xn}, b_{ym} and c_{mn} have to be determined. The number of terms in the above expressions (35) are necessarily truncated for practical matters. Obviously, the constants in (35) refer to a specific case and depend on the geometrical and constitutive characteristics of the cylinder, but above all on the entity of the angle α_0. As the applications in the following Sections 6 an 7 will show, the first constants are numerically more important. Typically, a large number of constants is not required to obtain an accurate displacement field. However, the number of constants increases if the angle α_0 increases and if the cross section is not very compact.

Using (35), the first and second partial derivatives of the three unknown functions can be computed. By substituting these derivatives in the field equations (12), the initial system of three partial differential equations is transformed into a system of three nonlinear algebraic equations, which we will denote with the following vectorial notation: $\mathbf{F}(\mathbf{x}) = \mathbf{0}$, where $\mathbf{x}$ is the vector of unknown constants. Similarly, the boundary conditions (13) can be rewritten as $\mathbf{g}(\mathbf{x}) = \mathbf{0}$ and (15) as $\mathbf{h}(\mathbf{x}) = \mathbf{0}$. Therefore, the boundary value problem simplifies in

$$\begin{cases} \mathbf{F}(\mathbf{x}) = \mathbf{0} & \text{in } \mathcal{B} \\ \mathbf{g}(\mathbf{x}) = \mathbf{0} & \text{in } \partial\mathcal{A} \text{ and } Z \in [0,\, L] \\ \mathbf{h}(\mathbf{x}) = \mathbf{0} & \text{in } \mathcal{A} \text{ and } Z = 0,\, L \end{cases} \tag{36}$$

To apply the numerical methods for solving problems (36), the domain $\mathcal{B}$ and its boundary $\partial\mathcal{B}$ are replaced with a grid of discrete points, in which all equations (36) will have collocation. Given the geometric symmetries of the cross section,

[17] Since all the cross sections undergo the same pure deformation, to better understand the symmetry properties of the unknown functions, it may be convenient to refer to the first cross section of the cylinder ($Z = 0$) which does not rotate.

only a quarter of it can be considered and discretized. The number of grid nodes can be increased as the angle α_0 increases.

Among the various numerical methods, Newton's method is one of the most popular [23]. It originates from the Taylor's series expansion about a point taking into account only the first order derivative. Newton's iterative formula applied to $(36)_1$ gives

$$\mathbf{x}^{(k+1)} = \mathbf{x}^{(k)} - \mathbf{J}_{\mathrm{F}}(\mathbf{x}^{(k)})^{-1}\mathbf{F}(\mathbf{x}^{(k)}), \tag{37}$$

where the index k represents the interation and $\mathbf{J}_{\mathrm{F}}$ is the Jacobian matrix. As the iterations begin to have the same repeated values, that is when $\mathbf{x}^{(k+1)} \cong \mathbf{x}^{(k)}$, the zeroes of the vector-valued function $\mathbf{F}(\mathbf{x})$ are found. Newton's method converges quadratically, and, in general, with this method the system converges quite rapidly once the approximation is close to the actual solution of the nonlinear system. At each iteration, (37) together with $(36)_2$ and $(36)_3$, constituting a nonlinear system for calculating the constant unknowns: a_{yn}, a_{xm}, b_{xn}, b_{ym}, c_{mn} and C. The total number of nodes in the grid, considering internal points and boundary points, must be equal to the number of constants to be calculated.[18]

To perform the analysis of the case studies reported in the next Sections 6 and 7, the solution provided by the linearized theory of torsion has been taken as starting point of the Newton's method. Then, the twist angle α_0 has been increased through steps of $\pi/10$, until convergence has been reached. On average, 10 iterations are requested to find the right coefficients in expressions (35) to satisfy system (36), with a prescribed tolerance of about 10^{-15} in all the collocation points. This iterative approach allows obtaining an accurate solution for the whole domain of the cylinder and for its boundary.

Definitely, expressions (35), with the constants determined with the iterative procedure, can be introduced in the displacement field (5) to obtain the equilibrium solution of non-circular cylinders subjected to large twisting. Once obtained a semi-analytic form of the displacement field (5), the deformation gradient $\mathbf{F}$ and the right Cauchy-Green strain tensor $\mathbf{C}$ can be calculated according to (7) and (8) for any point in the cylinder. Then, the Piola-Kirchhoff stress tensor $\mathbf{T}_R$ follows from (10). In this way, displacements, stretches and stresses for any point of the cylinder are determined.

By substituting the Piola-Kirchhoff stresses in equations (12), (13) and (15), a check about the accuracy of the solution obtained with the iterative procedure can be performed *a posteriori* by verifying that for each single equation the difference from zero is very small.

[18] When the numerical values of the unknown constants are too small, it is convenient to impose the boundary conditions not in local but in global form, obtaining average values.

6 Applications. The case of the elliptical cross section

For the first set of numerical computations a cylinder with elliptic cross section is considered. This cylinder has semi-diameters $A = 40$ [mm] and $B = 62.5$ [mm], and length L = 600 [mm]. The cylinder is made up of neoprene. For this type of material the following constitutive constants have recently been estimated [19]: $a = 456.9$, $b = 381.08$ and $c = 317.58$ [kPa]. In the following this example will be considered as the reference case study. For the overall torsion angle α_0 the following values are assumed: $\pi/4, \pi$ and 3π.

For the most severe situation, $\alpha_0 = 3\pi$, the application of the iterative procedure, described in the previous Section, provides the following expressions:

$$\begin{gathered} U(X,\,Y) \simeq \left(1 - 7.076 \cdot 10^{-6} Y^2 - 2.828 \cdot 10^{-9} Y^4\right) \left(0.91\, X + 5.305 \cdot 10^{-6} X^3 + 3.318 \cdot 10^{-9} X^5\right) - X; \\ V(X,\,Y) \simeq \left(1 - 6.464 \cdot 10^{-7} X^2 - 6.967 \cdot 10^{-9} X^4\right) \left(1.01\, Y - 1.614 \cdot 10^{-5} Y^3 + 1.009 \cdot 10^{-9} Y^5\right) - Y; \\ \psi(X,\,Y) \simeq -5.405 \cdot 10^{-3} XY - 3.257 \cdot 10^{-7} X^3 Y + 9.27 \cdot 10^{-8} XY^3. \end{gathered} \tag{38}$$

For the intermediate situation, $\alpha_0 = \pi$, the application of the iterative procedure provides the following expressions:

$$\begin{gathered} U(X,\,Y) \simeq \left(1 - 2.119 \cdot 10^{-6} Y^2\right) \left(0.988\, X + 1.809 \cdot 10^{-6} X^3\right) - X; \\ V(X,\,Y) \simeq \left(1 - 1.822 \cdot 10^{-6} X^2\right) \left(1.003\, Y - 1.572 \cdot 10^{-6} Y^3\right) - Y; \\ \psi(X,\,Y) \simeq -2.109 \cdot 10^{-3} XY - 1.706 \cdot 10^{-8} X^3 Y + 2.774 \cdot 10^{-9} XY^3. \end{gathered} \tag{39}$$

As regards the smallest angle, $\alpha_0 = \pi/4$, a situation for which linear theory cannot be applied anyway, the expressions are

$$\begin{gathered} U(X,\,Y) \simeq \left(1 - 1.679 \cdot 10^{-7} Y^2\right) X - X; \\ V(X,\,Y) \simeq \left(1 - 1.2512 \cdot 10^{-7} X^2\right) \left(Y - 9.919 \cdot 10^{-8} Y^3\right) - Y; \\ \psi(X,\,Y) \simeq -5.376 \cdot 10^{-4} XY. \end{gathered} \tag{40}$$

Note that $a_{x1} \gg a_{x2} \gg ..... \gg a_{xn}$; $a_{y1} \gg a_{y2} \gg ..... \gg a_{yn}$ and similarly for the other constants of (35). This shows that few terms are needed to accurately reproduce (even in the case of elongated sections and/or of large values of twisting) the three unknown functions. From the previous expressions also observe how fewer terms are needed to represent the unknown functions, always with a preassigned precision, as the angle α_0 is reduced.

The nine expressions (38), (39) and (40) are displayed in Fig. 4 using color maps. In the first row of the figure, Fig. 4(a), (b) and (c), the three unknown functions U, V and ψ are shown, in the same order, for the case with the smallest angle. The second row concerns the intermediate angle and the third the largest angle. The three functions plotted in each row of Fig. 4 are the same for all cross sections of the cylinder subjected to the prescribed torsion angle α_0. The first column of Fig. 4, i.e. Fig. 4(a), (d) and (g), shows the effects of the U function. The sections contract in the X direction losing the shape of the ellipse. These contributions to the in-plane displacement are very small for $\alpha_0 = \pi/4$, cf. Fig. 4(a) (in the linear theory they are identically null), and grow up to a

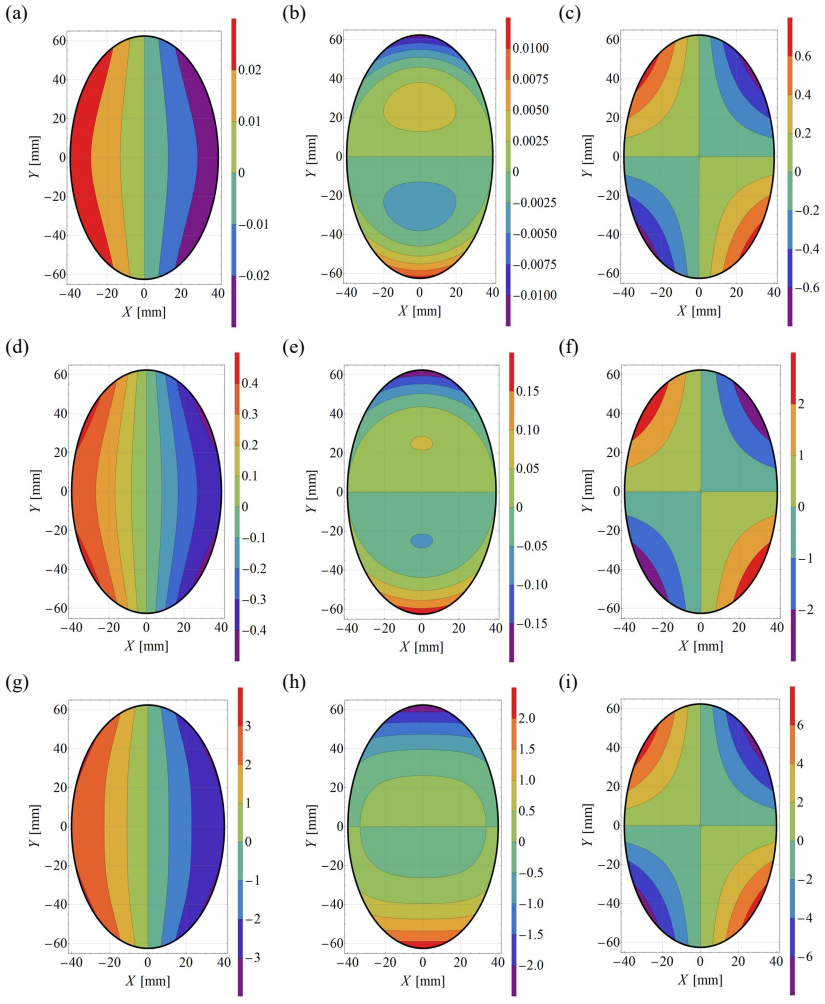

Figure 4: Plots of unknown functions, $U(X, Y)$, $V(X, Y)$ and $\psi(X, Y)$ (in [mm]), determined with the iterative procedure for the case study. (a), (b) and (c) Color maps of the expressions (40), $\alpha_0 = \pi/4$. (d), (e) and (f) Color maps of the expressions (39), $\alpha_0 = \pi$. (g), (h) and (i) Color maps of the expressions (38), $\alpha_0 = 3\pi$.

few millimeters for $\alpha_0 = 3\pi$, cf. Fig. 4(g). The maximum values occur at the ends of the smaller semi-diameter. The second column of Fig. 4, i.e. Fig. 4(b), (e) and (h), shows the effects of the V function. The sections contract in the Y direction losing the shape of the ellipse. These contributions to the in-plane displacement are very small for $\alpha_0 = \pi/4$, cf. Fig. 4(b) (in the linear theory they are identically null), and grow up to a few millimeters for $\alpha_0 = 3\pi$, cf. Fig. 4(h). The maximum values occur at the ends of the largest semi-diameter. The values of V are smaller than those of U, because the elliptical section has greater stiffness in the Y direction. The third column of Fig. 4, i.e. Fig. 4(c), (f) and (i), shows the planar projections of the warping function ψ. Geometrically, the warping function is a hyperbolic paraboloid (saddle). In absolute value, the maximum values of the warping function occur at the edge of the section and these increase as the torsion angle α_0 increases. In linear theory, the expression of the warping function for the elliptical section is (cf. (18))

$$\psi(X, Y) = -\frac{\alpha_0}{L}\frac{B^2 - A^2}{B^2 + A^2}XY. \tag{41}$$

For the case study with $\alpha_0 = \pi/4$, this formula provides $\psi(X, Y) = -5.483 \cdot 10^{-4}XY$, that is an expression close to $(40)_3$, highlighting how for small (but not infinitesimal) angles the expression of the linear theory retains a certain validity.

Fig. 5 illustrates the stretches λ_X, λ_Y and λ_Z, by means of color maps, for all points of a generic cross section of the cylinder (the tensor $\mathbf{C}$ does not depend on the variable Z). These stretches, plotted for each point of the cross section and for axes parallel to the axes of the reference system, are not principal, since the axes of the reference system adopted are not principal. The only exception is the centroid, where the stretches are principal. As in the previous figure, the images of the first row relate to the minor angle, those of the second row to the intermediate angle and those of the third row to the major angle. In the first column of Fig. 5, Fig. 5(a), (d) and (g), the λ_X values are shown. These are always less than one. The cross sections are contracted not uniformly, with the greatest contraction occurring in a central and vertical strip. For $\alpha_0 = \pi/4$, the values of λ_X are very close to one, namely to an undeformed situation, typical of linear theory. In the second column of Fig. 5, Fig. 5(b), (e) and (h), the values of the λ_Y stretch are shown. Except for a central area, where there is a slight dilatation, the sections are contracted. As in the case of the previous stretch, Fig. 5(b) also illustrates a practically undeformed situation. In the third column of Fig. 5, Fig. 5(c), (f) and (i), the λ_Z values are displayed. Since they are all greater than one, the stretches λ_Z show that there is non-uniform dilation in the direction of the cylinder axis. The maximum values occur at the ends of the major semi-diameter. Fig. 5(c) shows a slightly deformed situation. As the α_0 angle grows, however, these values become more important. To make the images of Fig. 5 more comprehensible, the graphs of the stretches along one of the two semi-diameters are also reported.

Among the six components of the Cauchy stress tensor $\mathbf{T}$,[19] the most im-

[19]The Cauchy stress tensor $\mathbf{T}$ does not depend on the variable Z. In this circumstance,

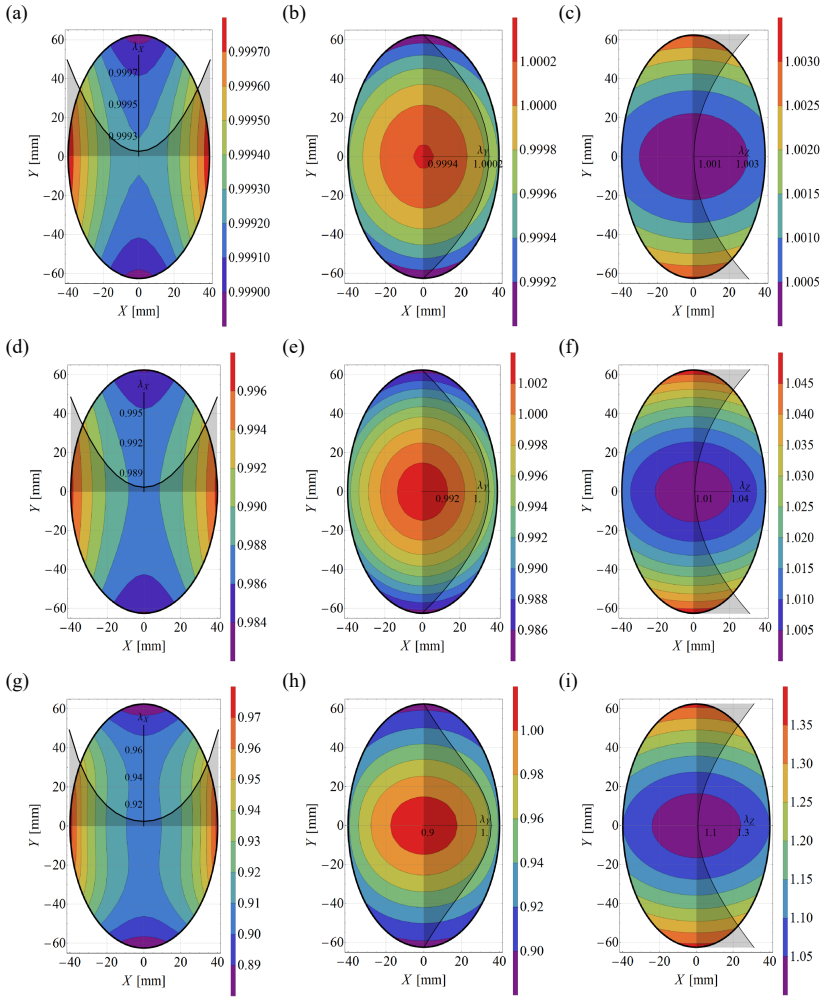

Figure 5: Plots of stretches for the case study. (a), (b) and (c) Color maps of λ_X, λ_Y and λ_Z respectively for $\alpha_0 = \pi/4$. (d), (e) and (f) Color maps of λ_X, λ_Y and λ_Z respectively for $\alpha_0 = \pi$. (g), (h) and (i) Color maps of λ_X, λ_Y and λ_Z respectively for $\alpha_0 = 3\pi$.

portant for the torsion problem are T_{xz} and T_{yz}. For the case study, these two components are illustrated in Fig. 6 for the usual three angles $\alpha_0 = \pi/4, \pi$ and 3π. As can be seen from Fig. 6(a) and (b), the stress diagrams have a shape similar to those of the linear theory, where the stresses are zero at the centroid and then grow linearly up to the outer edge of the section. By increasing the α_0 angle these diagrams take on curved shape as shown by Fig. 6(e) and (f). The maximum stress value always occurs at the outer end of the shortest semi-diameter.

The torsion moment m_t can be calculated with the following formula:

$$m_t = \int_{A'} (\mathrm{T}_{yz} x - \mathrm{T}_{xz} y)\, da. \tag{42}$$

The torsion moment is constant along the axis of the deformed cylinder. For the case study the variation of m_t with respect to the α_0 angle is shown in Fig. 7. As can be seen from this figure, initially the m_t graph is characterized by a quasi-linear law. As an alternative to applying the α_0 angle (boundary condition of geometric type), the twisting to the cylinder can be prescribed by the corresponding torsion moment m_t (boundary condition of static type).

Having finished the analysis of a compact elliptical section, we now turn to two limit situations, the elongated elliptical section and the circular section.

The following semi-diameters are assigned to the elongated elliptical section: $A = 25$ [mm] and $B = 100$ [mm]. In this way, the area of this new section is equal to that of the previous compact elliptical section. For the case with $\alpha_0 = \pi$, the iterative procedure provides the following expressions of the unknown functions:

$$\begin{aligned} U(X, Y) &\simeq \left(1 - 1.114 \cdot 10^{-5} Y^2\right) \left(0.997\, X + 3.086 \cdot 10^{-6} X^3\right) - X; \\ V(X, Y) &\simeq \left(1 + 1.796 \cdot 10^{-6} X^2\right) \left(1.008\, Y - 1.411 \cdot 10^{-6} Y^3\right) - Y; \\ \psi(X, Y) &\simeq -4.386 \cdot 10^{-3} XY - 5.36 \cdot 10^{-8} X^3 Y + 4.783 \cdot 10^{-8} XY^3. \end{aligned} \tag{43}$$

Using these expressions, the stretches and stresses were calculated and displayed in Fig. 8. Comparing the Fig. 8(a), (b) and (c) with the Fig. 5(d), (e) and (f), it can be seen that in the central part of the elongated section the stretches λ_X and λ_Y increase their values, evolving towards a situation with greater dilatation. Instead, the λ_Z stretch highlights how, unlike the previous case, the points belonging to this central area undergo a longitudinal shortening. A similar comparison for the stresses shows that the graph of the component T_{xz} along the y axis no longer has a quasi-linear trend.

By equating the area of the previously studied compact elliptical section with the area of a circular section, the radius of the latter is obtained: $R = 50$ [mm]. For the case with $\alpha_0 = \pi$, the iterative procedure provides the following expressions of the unknown functions:

$$\begin{aligned} U(X, Y) &\simeq \left(1 - 3.265 \cdot 10^{-7} Y^2\right) \left(0.994\, X - 3.246 \cdot 10^{-7} X^3\right) - X; \\ V(X, Y) &\simeq \left(1 - 3.265 \cdot 10^{-7} X^2\right) \left(0.994\, Y - 3.246 \cdot 10^{-7} Y^3\right) - Y; \\ \psi(X, Y) &\simeq 0. \end{aligned} \tag{44}$$

sometimes, the torsion is called uniform.

By interchanging the variables X and Y, the first two expressions have the same form. This is caused by the axisymmetry of the circular section. Furthermore, as is well known [12], for the circular section the warping function is zero. For this type of section, the longitudinal displacement field is uniform within each cross section and linearly variable along the axis of the cylinder. Using (44), the stretches and stresses were calculated and displayed in Fig. 9. Fig. 9(a) and (b) show the same graph for the λ_X and λ_Y stretches (moreover, this graph is the same also for each diameter of the cross section). Actually, the variations of these stretches in the cross section are very limited. The λ_X and λ_Y stretches show a slight non-uniform contraction of the section, likewise the longitudinal stretch λ_Z shows small elongations (cf. Fig. 9(c)). In [12], given its modest radial variation, the transversal stretch is assumed directly as a constant quantity. This assumption allows to obtain closed-form solutions. In particular, equations (28) and (25) of [12] give $\lambda = \lambda_X = \lambda_Y = 0.992$ and $\lambda_Z = 1.007$ for the points belonging to the axis of the cylinder.

At the end of this Section, a check can be carried out to evaluate the accuracy of the solution obtained. Having determined the Piola-Kirchhoff stress tensor, it can be verified whether the components of this tensor satisfy the equilibrium equations (12) and the boundary conditions (13) and (15). With reference to the first cross section of the cylinder ($Z = 0$), Fig. 10 shows the results of this analysis. The first three images of Fig. 10 show that the three components of $\mathrm{Div}\mathbf{T}_R$ are actually very close to zero at every point of the cross section.[20]

In the last three images of Fig. 10, the components of the stress vector along the edge of the section are plotted (given the symmetry only half the contour is drawn). As can be seen, these stress values are very small. In particular, the maximum deviation from zero is reached by the $\mathrm{t}_{R,Y}$ component, which numerically equals 3% of the maximum value of the stress component T_{yz}. The $\mathrm{t}_{R,Z}$ component is very small at the edge and is even smaller at the internal points of the section. Therefore, also the boundary condition (15) can be considered accurately satisfied.

Fig. 10 is plotted for the intermediate angle $\alpha_0 = \pi$. By increasing the α_0 angle until the case $\alpha_0 = 3\pi$, the situation just presented on the evaluation of the accuracy of the solution remains practically the same. It can therefore be concluded that the solution obtained satisfactorily meets the local equilibrium equations (12) and the boundary conditions (13) and (15).

7 Applications. The case of the rectangular cross section

In linear theory, the resolution of the boundary value problem (34) allows the computation of the warping function. In the case of the elliptical section, this

[20] For a comparison with scalar zero, the values of $\mathrm{Div}\mathbf{T}_R$ should be made dimensionless, for example by multiplying by a characteristic geometric dimension of the section and dividing by a stress value. However, considering the very low values of $\mathrm{Div}\mathbf{T}_R$, any normalization is omitted.

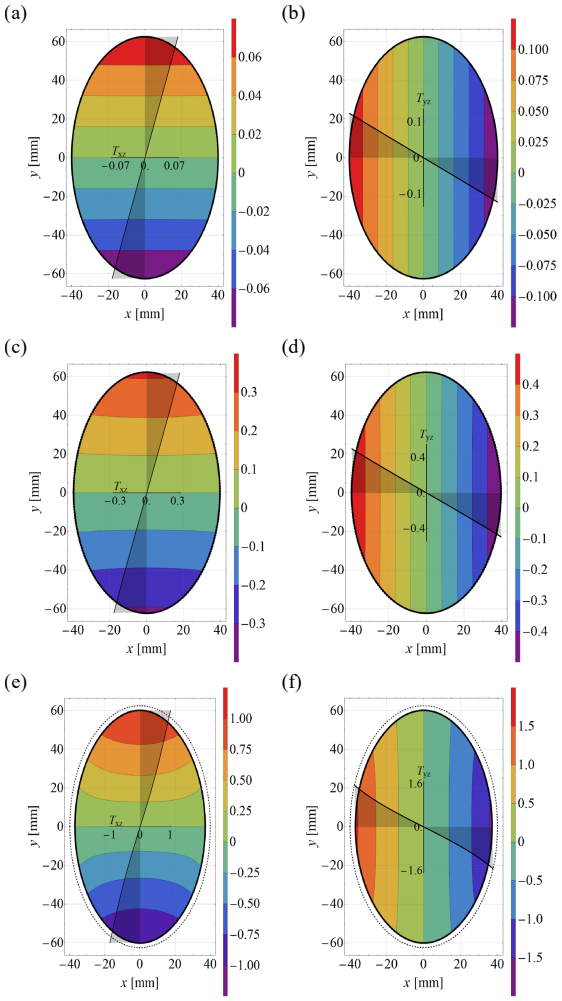

Figure 6: Plots of the Cauchy stresses (in [MPa]) for the case study. (a) and (b) Color maps of components T_{xz} and T_{yz} for $\alpha_0 = \pi/4$. (c) and (d) Color maps of components T_{xz} and T_{yz} for $\alpha_0 = \pi$. (e) and (f) Color maps of stress components T_{xz} and T_{yz} for $\alpha_0 = 3\pi$.

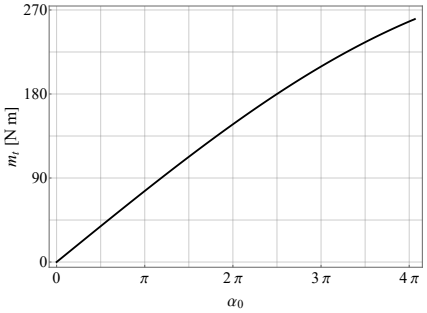

Figure 7: Torsion moment (in [Nm]) versus α_0 angle for the case study.

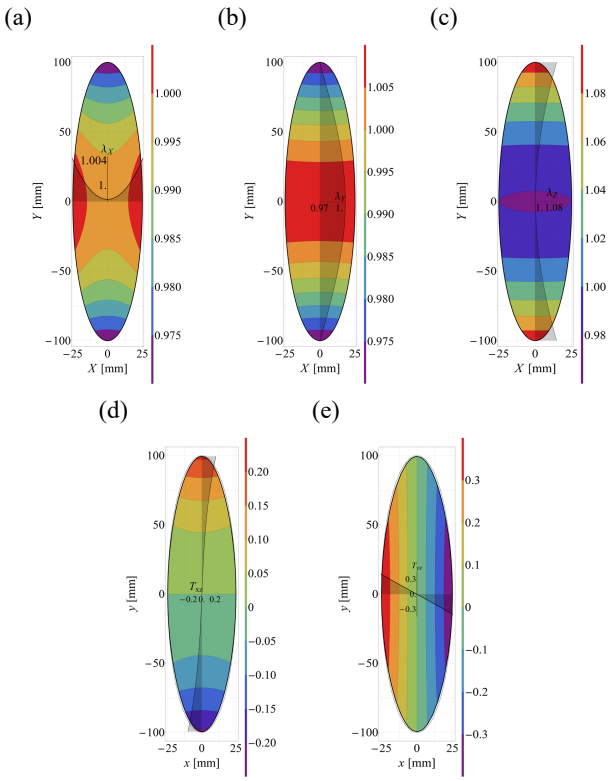

Figure 8: Plots of stretches and Cauchy stresses for the elongated elliptical section. Case with $\alpha_0 = \pi$. (a), (b) and (c) Color maps of λ_X, λ_Y and λ_Z respectively. (d) and (e) Color maps of stress components T_{xz} and T_{yz}.

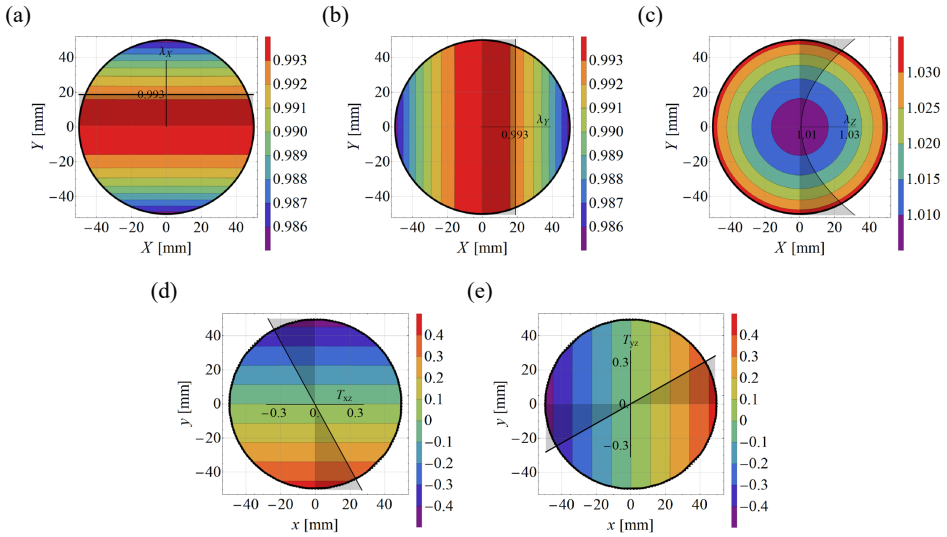

Figure 9: Plots of stretches and Cauchy stresses for the circular section. Case with $\alpha_0 = \pi$. (a), (b) and (c) Color maps of λ_X, λ_Y and λ_Z respectively. (d) and (e) Color maps of stress components T_{xz} and T_{yz}.

function can be obtained in closed form. As indicated by (41), it has the shape of a hyperbolic paraboloid. This no longer applies when switching to the rectangular section. The warping function in this case takes on a more complex form, and it is generally represented by a double power series. In the nonlinear theory, for any shape of the cross section, the warping function (cf. $(35)_3$), and consequently the equilibrium solution, is represented by power series.

The rectangular section is chosen in such a way as to circumscribe the previous compact elliptical section. Therefore, the cylinder has base $\bar{B} = 80$ [mm], height $\bar{H} = 125$ [mm] and length L = 600 [mm]. For the case with $\alpha_0 = \pi$, the iterative procedure provides the following expressions of the unknown functions:

$$\begin{aligned} U(X,\,Y) &\simeq \left(1 + 1.29 \cdot 10^{-6} Y^2\right)\left(0.987\,X - 3.143 \cdot 10^{-6} X^3\right) - X; \\ V(X,\,Y) &\simeq \left(1 + 1.363 \cdot 10^{-6} X^2\right)\left(1.006\,Y - 2.605 \cdot 10^{-6} Y^3\right) - Y; \\ \psi(X,\,Y) &\simeq -2.802 \cdot 10^{-3} XY - 7.071 \cdot 10^{-7} X^3 Y + 5.974 \cdot 10^{-7} X Y^3. \end{aligned} \tag{45}$$

Using these expressions, the stretches and stresses were calculated and displayed in Fig. 11. The rectangular section is more stiff than the elliptical, because it has more area, but certain similarities (also in numerical values) with Fig. 5(d), (e) and (f) and with Fig. 6(c) and (d) remain. In the rectangular section the stress diagrams traced for the two axes of the section always have a curved trendline. In the corners of the section the stresses tend to zero.

By equating the area of the previously studied rectangular section with the area of a square section, the side of the latter is obtained: $\tilde{A} = 100$ [mm]. For

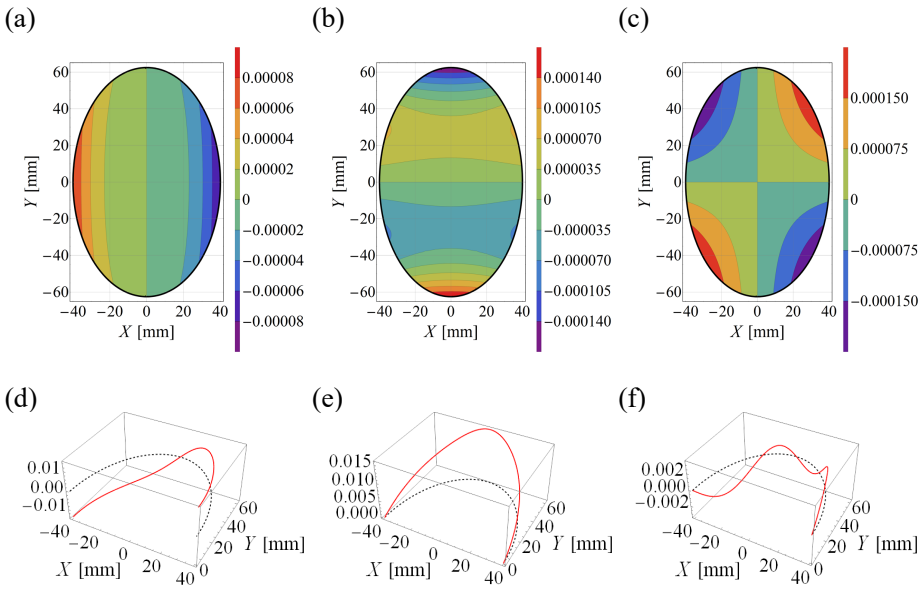

Figure 10: Accuracy of the equilibrium solution obtained for the compact elliptical section. Case with $\alpha_0 = \pi$. Color maps of components of vector field $\mathrm{Div}\mathbf{T}_R$. (a) Plot of the component $(\mathrm{Div}\mathbf{T}_R)_X$. (b) Plot of the component $(\mathrm{Div}\mathbf{T}_R)_Y$. (c) Plot of the component $(\mathrm{Div}\mathbf{T}_R)_Z$. Stress vector $\mathbf{t}_R$ at the boundary. (d) Plot of the component $\mathrm{t}_{R,X}$. (e) Plot of the component $\mathrm{t}_{R,Y}$. (f) Plot of the component $\mathrm{t}_{R,Z}$.

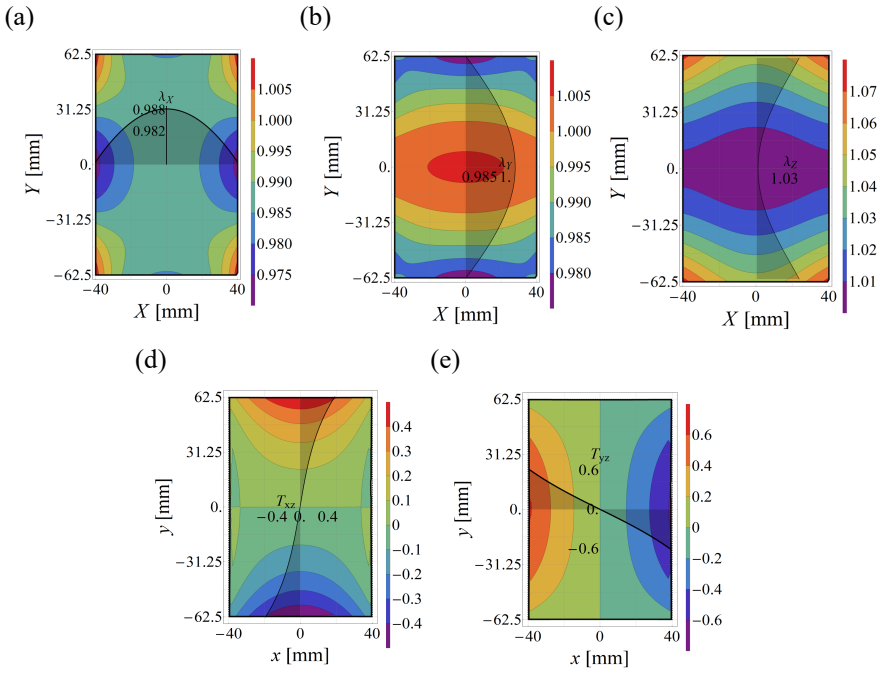

Figure 11: Plots of stretches and Cauchy stresses for the rectangular section. Case with $\alpha_0 = \pi$. (a), (b) and (c) Color maps of λ_X, λ_Y and λ_Z respectively. (d) and (e) Color maps of stress components T_{xz} and T_{yz}.

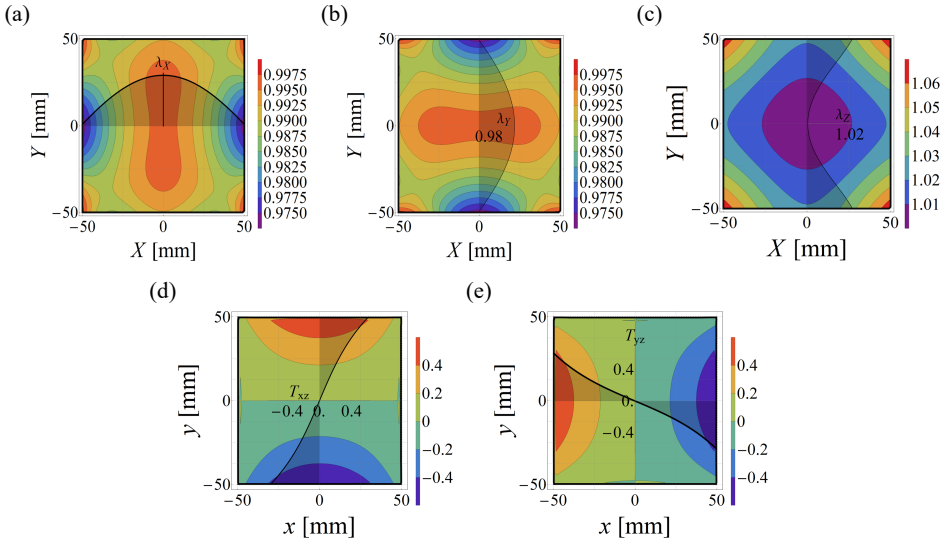

Figure 12: Plots of stretches and Cauchy stresses for the square section. Case with $\alpha_0 = \pi$. (a), (b) and (c) Color maps of λ_X, λ_Y and λ_Z respectively. (d) and (e) Color maps of stress components T_{xz} and T_{yz}.

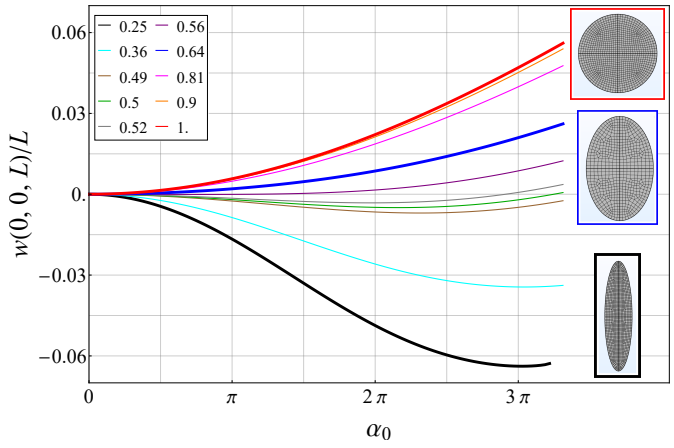

Figure 13: Poynting effect for the elliptical sections as a function of the prescribed angle of twist and for different ratio of the semi-diameters.

the case with $\alpha_0 = \pi$, the iterative procedure provides the following expressions of the unknown functions:

$$\begin{gathered} U(X,\,Y) \simeq \left(1 + 3.29 \cdot 10^{-6} Y^2\right)\left(0.996\,X - 3.052 \cdot 10^{-6} X^3\right) - X; \\ V(X,\,Y) \simeq \left(1 + 3.29 \cdot 10^{-6} X^2\right)\left(0.996\,Y - 3.052 \cdot 10^{-6} Y^3\right) - Y; \\ \psi(X,\,Y) \simeq -7.534 \cdot 10^{-7} X^3 Y + 7.534 \cdot 10^{-7} X Y^3. \end{gathered} \tag{46}$$

By interchanging the variables X and Y, the first two expressions have the same form, while the third changes only in sign. These symmetries are evident from the images of Fig. 12. The variations of the stretches λ_X and λ_Y are very limited, showing a slight contraction of the cross section, while the longitudinal stretch λ_Z points out small elongations, with values greater than one for each point of the section (cf. Fig. 12(c)).

8 The Poynting effect

Starting in 1909, for the finite torsion of steel wires and rubber cords, J. H. Poynting [13], [14] and [15], conducted experimental campaigns highlighting the appearance of normal longitudinal strains responsible for the sample elongation. This nonlinear aspect of the problem would later become known as the *Poynting effect*. In [12], for circular cylinders, it has been shown that a positive Poynting effect occurs, in the sense that increasing the twist angle also increases the elongation of the cylinder. The analysis developed in the present paper provides the possibility to investigate the influence of the shape of the cross section on the Poynting effect.

For sections with two axes of symmetry, in which the center of torsion coincides with the centroid, the Poynting effect is measured by the value of the longitudinal stretch λ_Z at the centroid of the cross section. For the uniform torsion problem (considered in this paper), the stretch λ_Z is constant along the torsion axis (i.e. it does not depend on the variable Z). As highlighted in the applications carried out in Sections 6 and 7, the centroidal stretch λ_Z can be greater or less than one. In particular, for compact sections it is greater than one (positive Poynting effect), while for elongated ones it can become less than one (negative Poynting effect).

By varying only the ratio between the semi-diameters, Fig. 13 shows the change in sign of the Poynting effect in the case of the elliptical section (the thick lines in Fig. 13 are related to the studied sections). Starting from the circular section, it can be seen that by increasing the torsion angle α_0, the axis of the cylinder lengthens and the same occurs for the axis of cylinders with compact elliptical section. Conversely, when the section has an elongated shape (ratio $A/B < 0.5$), by increasing the α_0 angle, the axis of the cylinder contracts. The change in sign of the Poynting effect, as the ratio between the semi-diameters of the ellipse varies, is thus highlighted.

Conclusions

In the fully nonlinear context of finite elasticity, this paper investigated the equilibrium problem of non-circular cylinders under torsion. This issue appears to have not been studied previously. One of the main difficulties lies in the fact that the cross sections of the cylinder, unlike the case with a circular section, now warp out of their plane.

Using the semi-inverse approach, a three-dimensional kinematic model has been defined, where, in addition to the rigid rotation of the cross sections, the large twist of the cylinder also generates in- and out-of-plane pure deformation of the cross sections and the change in length of the torsion axis. The displacement field prescribed by the kinematic model contains an unknown constant and three unknown functions. These functions depend on two variables and are used to describe the in-plane displacements of the cross sections and the out-of-plane displacements (warping function). The unknown constant physically represents the stretch of the torsion axis which governs the Poynting effect.

After calculating the deformation gradient and assuming the compressible Mooney-Rivlin form for the stored energy function, the Piola-Kirchhoff stress tensor has been derived. Then, the boundary value problem has been formulated for non-circular cylinders subjected to finite torsion. The first cross section of the cylinder is prevented from rotating (but can freely deform) and the last cross section undergoes the overall torsional rotation. Under these conditions, each section of the cylinder deforms in the same way (uniform torsion).

However, this equilibrium problem from a mathematical point of view takes on a complicated form. The field equations are a system of three partial differential equations of the second order in the three unknown functions, which depend on two variables. This system is strongly nonlinear and coupled, in the sense that all unknowns appear in each equation. Given its complexity, the boundary value problem formulated for the finite torsion of non-circular cylinders cannot be solved with standard analytical methods. Therefore, a specific solution technique for this class of problems has been proposed. The three unknown functions are developed in power series using polynomial terms in two variables. All constants of the above three series are evaluated through a iterative procedure based on Newton's method. Assessed the constants, the displacement field can be expressed in a semi-analytical form and, successively, deformation and stress tensors can be directly computed. The Piola-Kirchhoff stress tensor, thus evaluated, can therefore be substituted into all the equations of the boundary value problem and a checking of the accuracy of the solution obtained can be carried out *a posteriori*.

Invoking the hypotheses of smallness of both the deformation and displacement fields, and using Navier's classical linear constitutive law, the theory exposed for the finite torsion has been linearized, retrieving the classical results of the linear theory for non-circular cylinders.

Numerous applications have been carried out for cylinders with circular, elliptical (both compact and elongated), square and rectangular base. For each single case the three unknown functions, the stretches and the Cauchy stresses

were evaluated. The most important results were shown in graphs using color maps. The numerical verifications of the accuracy of the equilibrium solutions obtained gave very satisfactory results.

A specific study on the Poynting effect has shown that it is positive (the torsion axis lengthens) in the case of compact sections, whereas it becomes negative (the torsion axis contracts) in the case of elongated sections.

Acknowledgment Financial support from the Italian Ministry of Education, University and Research (MIUR) in the framework of the Project FISR 2019: "Eco Earth" (code 00245) is gratefully acknowledged. Financial support from University of Modena and Reggio Emilia in the framework of "FAR Dipartimentale 2020" (CUP E92F20000640001) is gratefully acknowledged.

Appendix. Components of the Piola-Kirchhoff stress tensor

Using (7), (8), (11) and (17), the components of the Piola-Kirchhoff stress tensor (10) assume the following expressions:

$$
\begin{aligned}
\mathrm{T}_{R_{11}} &= 2\left[(1+U_{,X})\cos\theta_1 Z - V_{,X}\sin\theta_1 Z\right](\omega_{,1}+I_1\omega_{,2})\\
&-2\left\{\left[(1+U_{,X})\cos\theta_1 Z - V_{,X}\sin\theta_1 Z\right]\left[(1+U_{,X})^2+V_{,X}^2+\psi_{,X}^2\right]\right\}\omega_{,2}\\
&-2\left\{\left[U_{,Y}\cos\theta_1 Z-(1+V_{,Y})\sin\theta_1 Z\right]\left[(1+U_{,X})U_{,Y}+(1+V_{,Y})V_{,X}+\psi_{,X}\psi_{,Y}\right]\right\}\omega_{,2}\\
&+2\left\{\theta_1\left[(X+U)\sin\theta_1 Z+(Y+V)\cos\theta_1 Z\right]\left[-\theta_1(1+U_{,X})(Y+V)+\theta_1(X+U)V_{,X}+C\psi_{,X}\right]\right\}\omega_{,2}\\
&+2\left\{C\left[U_{,Y}\sin\theta_1 Z+(1+V_{,Y})\cos\theta_1 Z\right]-\psi_{,Y}\theta_1\left[(X+U)\cos\theta_1 Z-(Y+V)\sin\theta_1 Z\right]\right\}I_3\omega_{,3}\tfrac{1}{\det\mathbf{F}},
\end{aligned}
$$

$$
\begin{aligned}
\mathrm{T}_{R_{12}} &= 2\left[U_{,Y}\cos\theta_1 Z-(1+V_{,Y})\sin\theta_1 Z\right](\omega_{,1}+I_1\omega_{,2})\\
&-2\left\{\left[(1+U_{,X})\cos\theta_1 Z - V_{,X}\sin\theta_1 Z\right]\left[(1+U_{,X})U_{,Y}+(1+V_{,Y})V_{,X}+\psi_{,X}\psi_{,Y}\right]\right\}\omega_{,2}\\
&-2\left\{\left[U_{,Y}\cos\theta_1 Z-(1+V_{,Y})\sin\theta_1 Z\right]\left[U_{,Y}^2+(1+V_{,Y})^2+\psi_{,Y}^2\right]\right\}\omega_{,2}\\
&+2\left\{\theta_1\left[(X+U)\sin\theta_1 Z+(Y+V)\cos\theta_1 Z\right]\left[-\theta_1(Y+V)U_{,Y}+\theta_1(X+U)(1+V_{,Y})+C\psi_{,Y}\right]\right\}\omega_{,2}\\
&+2\left\{-C\left[(1+U_{,X})\sin\theta_1 Z+V_{,X}\cos\theta_1 Z\right]+\psi_{,X}\theta_1\left[(X+U)\cos\theta_1 Z-(Y+V)\sin\theta_1 Z\right]\right\}I_3\omega_{,3}\tfrac{1}{\det\mathbf{F}},
\end{aligned}
$$

$$
\begin{aligned}
\mathrm{T}_{R_{13}} &= -2\theta_1\left[(X+U)\sin\theta_1 Z+(Y+V)\cos\theta_1 Z\right](\omega_{,1}+I_1\omega_{,2})\\
&-2\left\{\left[(1+U_{,X})\cos\theta_1 Z - V_{,X}\sin\theta_1 Z\right]\left[-\theta_1(1+U_{,X})(Y+V)+\theta_1(X+U)V_{,X}+C\psi_{,X}\right]\right\}\omega_{,2}\\
&-2\left\{\left[U_{,Y}\cos\theta_1 Z-(1+V_{,Y})\sin\theta_1 Z\right]\left[-\theta_1(Y+V)U_{,Y}+\theta_1(X+U)(1+V_{,Y})+C\psi_{,Y}\right]\right\}\omega_{,2}\\
&+2\left\{\theta_1\left[(X+U)\sin\theta_1 Z+(Y+V)\cos\theta_1 Z\right]\left[\theta_1^2\left[(X+U)^2+(Y+V)^2\right]+C^2\right]\right\}\omega_{,2}\\
&+2\left\{\psi_{,Y}\left[(1+U_{,X})\sin\theta_1 Z+V_{,X}\cos\theta_1 Z\right]-\psi_{,X}\left[U_{,Y}\sin\theta_1 Z+(1+V_{,Y})\cos\theta_1 Z\right]\right\}I_3\omega_{,3}\tfrac{1}{\det\mathbf{F}},
\end{aligned}
$$

$$
\begin{aligned}
\mathrm{T}_{R_{21}} &= 2\left[(1+U_{,X})\sin\theta_1 Z+V_{,X}\cos\theta_1 Z\right](\omega_{,1}+I_1\omega_{,2})\\
&-2\left\{\left[(1+U_{,X})\sin\theta_1 Z + V_{,X}\cos\theta_1 Z\right]\left[(1+U_{,X})^2+V_{,X}^2+\psi_{,X}^2\right]\right\}\omega_{,2}\\
&-2\left\{\left[U_{,Y}\sin\theta_1 Z+(1+V_{,Y})\cos\theta_1 Z\right]\left[(1+U_{,X})U_{,Y}+(1+V_{,Y})V_{,X}+\psi_{,X}\psi_{,Y}\right]\right\}\omega_{,2}\\
&-2\left\{\theta_1\left[(X+U)\cos\theta_1 Z-(Y+V)\sin\theta_1 Z\right]\left[-\theta_1(1+U_{,X})(Y+V)+\theta_1(X+U)V_{,X}+C\psi_{,X}\right]\right\}\omega_{,2}\\
&+2\left\{-C\left[U_{,Y}\cos\theta_1 Z-(1+V_{,Y})\sin\theta_1 Z\right]-\psi_{,Y}\theta_1\left[(X+U)\sin\theta_1 Z+(Y+V)\cos\theta_1 Z\right]\right\}I_3\omega_{,3}\tfrac{1}{\det\mathbf{F}},
\end{aligned}
$$

$$
\begin{array}{c}
\mathrm{T}_{R_{22}} = 2\left[U_{,Y}\sin\theta_1 Z + (1+V_{,Y})\cos\theta_1 Z\right](\omega_{,1} + I_1\omega_{,2}) \\
-2\left\{\left[(1+U_{,X})\sin\theta_1 Z + V_{,X}\cos\theta_1 Z\right]\left[(1+U_{,X})U_{,Y} + (1+V_{,Y})V_{,X} + \psi_{,X}\psi_{,Y}\right]\right\}\omega_{,2} \\
-2\left\{\left[U_{,Y}\sin\theta_1 Z + (1+V_{,Y})\cos\theta_1 Z\right]\left[U_{,Y}^2 + (1+V_{,Y})^2 + \psi_{,Y}^2\right]\right\}\omega_{,2} \\
-2\left\{\theta_1\left[(X+U)\cos\theta_1 Z - (Y+V)\sin\theta_1 Z\right]\left[-\theta_1(Y+V)U_{,Y} + \theta_1(X+U)(1+V_{,Y}) + C\psi_{,Y}\right]\right\}\omega_{,2} \\
+2\left\{C\left[(1+U_{,X})\cos\theta_1 Z - V_{,X}\sin\theta_1 Z\right] + \psi_{,X}\theta_1\left[(X+U)\sin\theta_1 Z + (Y+V)\cos\theta_1 Z\right]\right\} I_3\omega_{,3}\frac{1}{\det\mathbf{F}},
\end{array}
$$

$$
\begin{array}{c}
\mathrm{T}_{R_{23}} = 2\theta_1\left[(X+U)\cos\theta_1 Z - (Y+V)\sin\theta_1 Z\right](\omega_{,1} + I_1\omega_{,2}) \\
-2\left\{\left[(1+U_{,X})\sin\theta_1 Z + V_{,X}\cos\theta_1 Z\right]\left[-\theta_1(1+U_{,X})(Y+V) + \theta_1(X+U)V_{,X} + C\psi_{,X}\right]\right\}\omega_{,2} \\
-2\left\{\left[U_{,Y}\sin\theta_1 Z + (1+V_{,Y})\cos\theta_1 Z\right]\left[-\theta_1(Y+V)U_{,Y} + \theta_1(X+U)(1+V_{,Y}) + C\psi_{,Y}\right]\right\}\omega_{,2} \\
-2\left\{\theta_1\left[(X+U)\cos\theta_1 Z - (Y+V)\sin\theta_1 Z\right]\left[\theta_1^2\left[(X+U)^2 + (Y+V)^2\right] + C^2\right]\right\}\omega_{,2} \\
+2\left\{-\psi_{,Y}\left[(1+U_{,X})\cos\theta_1 Z - V_{,X}\sin\theta_1 Z\right] + \psi_{,X}\left[U_{,Y}\cos\theta_1 Z - (1+V_{,Y})\sin\theta_1 Z\right]\right\} I_3\omega_{,3}\frac{1}{\det\mathbf{F}},
\end{array}
$$

$$
\begin{array}{c}
\mathrm{T}_{R_{31}} = 2\psi_{,X}(\omega_{,1} + I_1\omega_{,2}) \\
-2\left\{\psi_{,X}\left[(1+U_{,X})^2 + V_{,X}^2 + \psi_{,X}^2\right]\right\}\omega_{,2} \\
-2\left\{\psi_{,Y}\left[(1+U_{,X})U_{,Y} + (1+V_{,Y})V_{,X} + \psi_{,X}\psi_{,Y}\right]\right\}\omega_{,2} \\
-2\left\{C\left[-\theta_1(1+U_{,X})(Y+V) + \theta_1(X+U)V_{,X} + C\psi_{,X}\right]\right\}\omega_{,2} \\
+2\left\{\theta_1\left[(X+U)U_{,Y} + (Y+V)(1+V_{,Y})\right]\right\} I_3\omega_{,3}\frac{1}{\det\mathbf{F}},
\end{array}
$$

$$
\begin{array}{c}
\mathrm{T}_{R_{32}} = 2\psi_{,Y}(\omega_{,1} + I_1\omega_{,2}) \\
-2\left\{\psi_{,X}\left[(1+U_{,X})U_{,Y} + (1+V_{,Y})V_{,X} + \psi_{,X}\psi_{,Y}\right]\right\}\omega_{,2} \\
-2\left\{\psi_{,Y}\left[U_{,Y}^2 + (1+V_{,Y})^2 + \psi_{,Y}^2\right]\right\}\omega_{,2} \\
-2\left\{C\left[-\theta_1(Y+V)U_{,Y} + \theta_1(X+U)(1+V_{,Y}) + C\psi_{,Y}\right]\right\}\omega_{,2} \\
+2\left\{-\theta_1\left[(X+U)(1+U_{,X}) + (Y+V)V_{,X}\right]\right\} I_3\omega_{,3}\frac{1}{\det\mathbf{F}},
\end{array}
$$

$$
\begin{array}{c}
\mathrm{T}_{R_{33}} = 2C(\omega_{,1} + I_1\omega_{,2}) \\
-2\left\{\psi_{,X}\left[-\theta_1(1+U_{,X})(Y+V) + \theta_1(X+U)V_{,X} + C\psi_{,X}\right]\right\}\omega_{,2} \\
-2\left\{\psi_{,Y}\left[-\theta_1(Y+V)U_{,Y} + \theta_1(X+U)(1+V_{,Y}) + C\psi_{,Y}\right]\right\}\omega_{,2} \\
-2\left\{C\left[\theta_1^2\left[(X+U)^2 + (Y+V)^2\right] + C^2\right]\right\}\omega_{,2} \\
+2\left\{(1+U_{,X})(1+V_{,Y}) - U_{,Y}V_{,X}\right\} I_3\omega_{,3}\frac{1}{\det\mathbf{F}},
\end{array}
\tag{47}
$$

where $\omega_{,i} = \frac{\partial\omega}{\partial I_i}$, for $i = 1, 2$ and 3. The last three components do not depend on the variable Z.

References

[1] C.A. Coulomb, Recherches théoriques et expérimentales sur la force de torsion, et sur l'élasticité d es fils de métal. *Histoire de l'Académie*, Paris (1784) 229-269.

[2] A.J.C Barré de Saint-Venant, Mémoire sur la torsion des prismes. *Mémoire de l'Acad. Savants étrangers* **14** (1855) 233-560.

[3] A.J.C Barré de Saint-Venant, Sur une formule donnant approximativement le moment de torsion. *Comptes Rendus* **88** (1879) 142-147.

[4] L.M.B.C. Campos, F.S.R.P. Cunha, On the torsion of a prism with non-equilateral triangular cross-section. *Inter. J. of Eng. Science.* **48** (2010) 718-725.

[5] J. Francu, P. Novàckovà, P. Janıcek, Torsion of a non-circular bar. *Engineering Mechanics* **19** (2012) 45 -60.

[6] K. Abdelkader, Z. Toufik, B.J. Mohamed, Torsional stress in non-circular cross sections by the finite element method. *Advances in Mechanical Engineering* **7** (2015) 1-20. DOI: 10.1177/1687814015581979.

[7] K. Bhaskar, T.K. Varadan, *Torsion of Non-circular Sections. In: Theory of Isotropic/Orthotropic Elasticity.* Springer (2023) Cham. https://doi.org/10.1007/978-3-031-06345-9_4.

[8] B.R. Seth, Finite strain in elastic problems. *Phil. Trans. Roy. Soc. of London. Series A, Math. and Phys. Sciences* **234** (1935) 231–264.

[9] R.S. Rivlin, Large elastic deformations of isotropic materials. III. Some simple problems in cylindrical polar co-ordinates. *Phil. Trans. Roy. Soc.* A **240** (1948) 509-525.

[10] R.S. Rivlin, Large elastic deformation of isotropic materials. IV. Further developments of the general theory. *Phil. Trans. Roy. Soc.* A **241** (1948) 379-397.

[11] R.S. Rivlin, Large elastic deformation of isotropic materials. VI. Further results in the theory of torsion, shear and flexure. *Phil. Trans. Roy. Soc.* A **242** (1949) 173-195.

[12] F.O. Falope, L. Lanzoni, A. M. Tarantino, Finite torsion of compressible circular cylinders: An approximate solution. *J. Elasticity* **151** (2022) 187-217.

[13] J.H. Poynting, The wave motion of a revolving shaft, and a suggestion as to the angular momentum in a beam of circularly polarised light. *Proc. Roy. Soc. of London.* A **82** (1909) 560-567.

[14] J.H. Poynting, On the changes in the dimensions of a steel wire when twisted, and on the pressure of distortional waves in steel. *Proc. Roy. Soc. of London.* A **86** (1912) 534-561.

[15] J.H. Poynting, The changes in length and volume of an Indian-rubber cord when twisted. *India-Rubber J.* October, 4 (1913) p. 6.

[16] L. Lanzoni, A.M. Tarantino, Finite anticlastic bending of hyperelastic solids and beams. *J. Elasticity* **131** (2018) 137-170.

[17] L. Lanzoni. A.M. Tarantino. The bending of beams in finite elasticity. *J. Elasticity* **139** (2020) 91-121.

[18] L. Lanzoni. A.M. Tarantino. Mechanics of High-Flexible Beams under Live Loads. *J. Elasticity* **140** (2020) 95-125.

[19] F.O. Falope, L. Lanzoni, A. M. Tarantino, The bending of fully nonlinear beams. Theoretical, numerical and experimental analyses. *Inter. J. of Eng. Science.* **145** (2019) 103167.

[20] M. Pelliciari, S. Sirotti, A.M. Tarantino, A strain energy fuction for large deformations of compressible elastomers. *J.Mech. Phys. Solids* (2023) 105308.

[21] M. Pelliciari, A.M. Tarantino, Equilibrium paths for Von Mises trusses in finite elasticity. *J. Elasticity* **138** (2020) 145-168.

[22] M. Pelliciari, A.M. Tarantino, Equilibrium and Stability of Anisotropic Hyperelastic Graphene Membranes. *J. Elasticity* 144 (2021) 169-195.

[23] R.L. Burden, J.D. Faires. *Numerical Analysis. Numerical solution of Nonlinear System of Equations.* Belmount Brooks/Cole (2005) 597-640.